Escola d'Enginyeria de Telecomunicació i Aeroespacial de Castelldefels
UNIVERSITAT POLITÈCNICA DE CATALUNYA

MASTER THESIS

TITLE: Powering autonomous sensors by RF harvesting

MASTER DEGREE: Master of Science in Telecommunication Engineering & Management

AUTHORS: David Jiménez López
Iker Antxustegi-etxearte Atienzar

DIRECTOR: Manel Gasulla Forner

DATE: September 13th 2013

Overview

RF energy can be harvested in order to power autonomous sensors either from the surrounding environment or from dedicated sources. A conventional RF harvester is mainly composed by an antenna, a matching network and a rectifier. At low power level, e.g. -10 dBm and below, the corresponding voltage amplitude at the antenna is low and comparable to the voltage drop of the diodes used in the rectifier. Two matching network configuration are compared in terms of efficiency, a shunt-inductor and an L-network. Then, in order to boost the voltage at the rectifier input and thus the rectifier efficiency, an L-network optimized for an input power of -10 dBm at 868 MHz is proposed in this work. As for the rectifier, a half-wave rectifier with a single zero-bias Schottky diode HSMS2820 was selected for high powers (≥5 dBm) and HSMS2850 for low powers (<5 dBm). First, a theoretical analysis was performed that takes into account the parasitic capacitance of the diode. Then, simulations with ADS (Harmonic Balance) were carried out taking into account the circuit layout. Both in the analysis and simulations, the antenna was substituted by an AC generator with an output resistance of both 50 Ω and 300Ω. Finally, a printed circuit board (PCB) implementation was performed using a 0.5 pF capacitor and a 27 nH inductor for the L-network. First, the input power was generated by an RF generator and directly connected to the circuit. The RF-to-DC efficiency was of 45 % at 868 MHz with an optimum load of 2.5 kΩ. Efficiencies of 34.5 % and 22.5 % were achieved at -15 dBm and -20 dBm, respectively. Ultimately, two antennas have been manufactured at the resonant frequency of the system in order to implement a real system. The RF-to-DC efficiency was of 41.85 % at 868 MHz with an optimum load of 4 kΩ and efficiencies of 29.42 % and 19.73 % were achieved at -15 dBm and -20 dBm, respectively.

INDEX

INTRODUCTION

This project reports the design, simulation, implementation, and testing of a radiofrequency (RF) energy harvester. Powering autonomous sensors from electromagnetic waves has been proposed in the literature [1]-[4]-[6]. A conventional RF harvester is mainly composed by an antenna, a matching network and a rectifier. Reported RF-to-DC power efficiencies are higher for increasing power levels at the RF input. In [6], efficiencies around 70 % and 40 % are achieved for RF power levels of 10 dBm and -10 dBm, respectively. The circuits and diodes used for each power range are different in order to optimize the performance.

This work focuses on the matching network stage in order to achieve high efficiencies at low input power levels, in particular at -10 dBm. At this power level, the corresponding voltage amplitude at the antenna is low and comparable to the voltage drop of the diodes used in the rectifier. So, in order to increase the rectifier efficiency, a boost of the antenna voltage is required before driving the rectifier. Here, a high-Q L-network is proposed with a resonant frequency of 868 MHz (ISM band). As the voltage is boosted by the matching network there is no need to further boost it by using the rectifier and thus a single-diode half-wave rectifier was used.

First chapter presents the project background. Then, second chapter performs a theoretical analysis that takes into account the parasitic capacitance of the diode rectifier. A zero-bias Schottky diode HSMS2820 and HSMS2850 comparison was done. Third chapter shows simulations with ADS (Harmonic Balance) with actual components and rectifier model. Finally, chapter 4 shows simulations taking into account the circuit layout and the printed circuit board (PCB) implementation. First, the antenna was simulated by an RF generator with an output impedance of 50 Ω. Then, a real antenna implementation was performed. Efficiency measurements of both configurations were taken. The selected components for the L-network were a 0.5 pF capacitor and a 27 nH inductor.

CHAPTER 1. BACKGROUND

Autonomous sensor is becoming an increasingly used solution. The reduction in the power consumption has contributed on it. Power supply is one of the autonomous sensor challenges. This project is focus on power supply for low-power autonomous sensors through RF energy.

This chapter briefly describes autonomous sensors, different options for their power supply and a general overview of RF harvesting. Besides, microstrip transmission lines are briefly explained.

1.1. Autonomous sensors

Autonomous sensors are used in numerous fields, including healthcare, aerospace, and environmental monitoring. An autonomous sensor is a device that converts a signal from a physical or chemical quantity to a corresponding signal in the electrical domain. The main difference with conventional sensors is that an autonomous sensor can perform its tasks without being connected. Its power supply stage is integrated in the device and the data information is transmitted wirelessly. Power can be provided either by primary batteries or by harvesting the energy from the ambient. In order to save power, autonomous sensors are in sleep mode (standby) most of the time, and only wake up when needs to take measurements, processing and transmission/reception of data.

Fig. 1.1 shows the block diagram of an autonomous sensor, including the power supply subsystem.

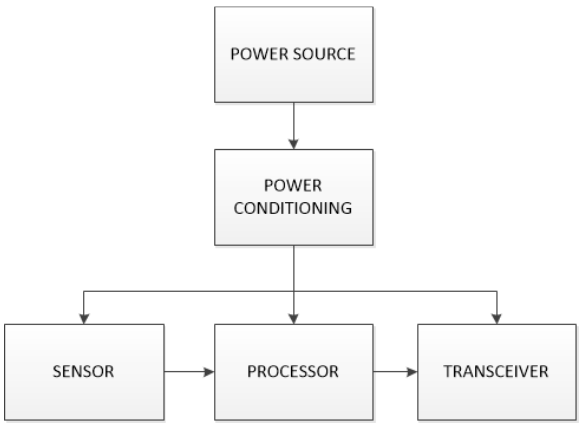

Fig. 1.1. Block diagram of an autonomous sensor.

In this project only the power source stage has been studied. The power conditioning stage depends on each sensor and matches the power source at the power requirements of the load. The other stages; sensor, processor and transceiver, are neither studied nor explained. More information about it is found at [1].

Regarding with power sources, in this project RF energy harvesting is considered. The main advantage over batteries is that it enables autonomous sensors to run in nearly perpetual operation with little or no maintenance. However, it increases circuit complexity and is a fledgling technology that still poses certain challenges.

1.1.1. Ambient energy sources

Certainly, solar and wind energy are the most popular renewable energy sources. However, there are several ambient energy sources that could be useful to power autonomous sensors, among them [1]: Radiant, mechanical, thermal, magnetic and biochemical.

Radiofrequency energy (a specific type of radiant energy) has been considered in this project and it is explained in detail in next section.

1.2. Radiofrequency energy harvesting

The radiofrequency (RF) energy is continually radiated by mobile phone stations and broadcasting station antennas. Different polarizations and a broad range of frequencies are used from RF signals. Although, there are a multiple antennas radiating RF energy, the power level from ambient RF sources are low [3]. In this way, a good RF harvesting system design is required to take the maximum advantage of low power levels.

On the other hand, energy can also be deliberately radiated without license on the industrial, scientific and medical (ISM) applications frequency bands. The power density (*S*) can be obtained from the following equation:

$$S = P_{\mathrm{EIRP}}/4\pi d^2 \qquad (1.1)$$

Whereby P_{EIRP} is the effective isotropically radiated power from the transmitter and d is the distance between transmitter and receiver. This case is for free-space propagation losses; for other scenarios, the power decays with other factor, typically higher. In urban ambient there are other factors that affect *S*, such as multipath propagation and reflections; thus, calculating the real *S* for an urban location requires accurate simulations or field measurements. The available power from the antenna (P_{av}) depends

on *S* and on the effective aperture (area) of the antenna (A_{e}), as shown below (known as the Friis relation):

$$P_{\mathrm{av}} = S \cdot A_{\mathrm{e}} = S \cdot \frac{\lambda_{\mathrm{RF}}^2}{4\pi} G_{\mathrm{r}} = P_{\mathrm{EIRP}} G_{\mathrm{r}} \frac{\lambda_{\mathrm{RF}}^2}{(4\pi d)^2} \tag{1.2}$$

Whereby $A_{\mathrm{e}} = \lambda_{\mathrm{RF}}^2 \cdot G_{\mathrm{r}}/4\pi$; G_{r} is the antenna gain; and λ_{RF} is the wavelength. Equation (1.2), only valid for free space propagation losses, clearly demonstrates that the higher the frequency (λ_{RF} is inversely proportional to frequency), the lower the powering range. In Europe, there are several frequency bands for ISM applications, being 433 MHz, 868 MHz and 2.4 GHz the most popular. Here, RF harvesting in ISM bands is considered and the 868 MHz band is chosen as a trade-off between, the antenna size and the powering range. The maximum P_{EIRP} for ISM frequency bands in Europe is regulated by European Communications Office (ECO). In the 868 MHz band the maximum P_{EIRP} allowed is 500 mW [16].

Fig. 1.2 shows the building blocks of an RF energy harvester, encompassing an antenna, an impedance matching block and a rectifier. These blocks are described below:

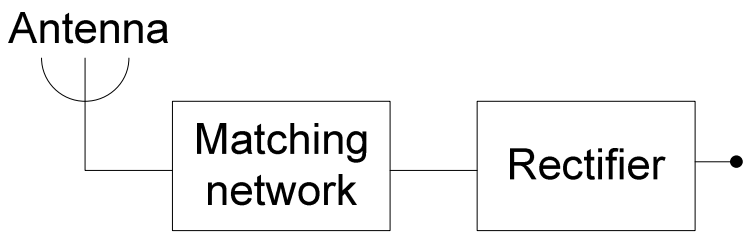

Fig. 1.2. RF energy harvester scheme.

1.2.1. Antenna

The first stage of any RF energy harvester system is an antenna. It carries out the conversion of electromagnetic waves to electric power and vice versa. An antenna can be represented as an AC voltage source (V_{s}) with a series impedance (see Fig. 1.3). This series impedance is formed by a resistive and a reactive part. The resistive part basically comprises the radiation resistance (R_{s}), which is a virtual resistance that emulates the transmitted or received power from the electromagnetic wave, and the loss resistance (R_{loss}), which appears from the actual resistance of the elements that form the antenna (e.g. copper) and the dielectric losses. R_{loss} is low at DC but it can

increase at high frequencies, due to the skin effect. All the power dissipated on R_{loss} is wasted. In this project R_{loss} is not considered because, at 868 MHz (frequency used) R_{loss} is small compared to R_{s}. The reactive part is formed by jX_{ant}. Depending on the antenna design, X_{ant} can be either positive (inductive) or negative (capacitive).

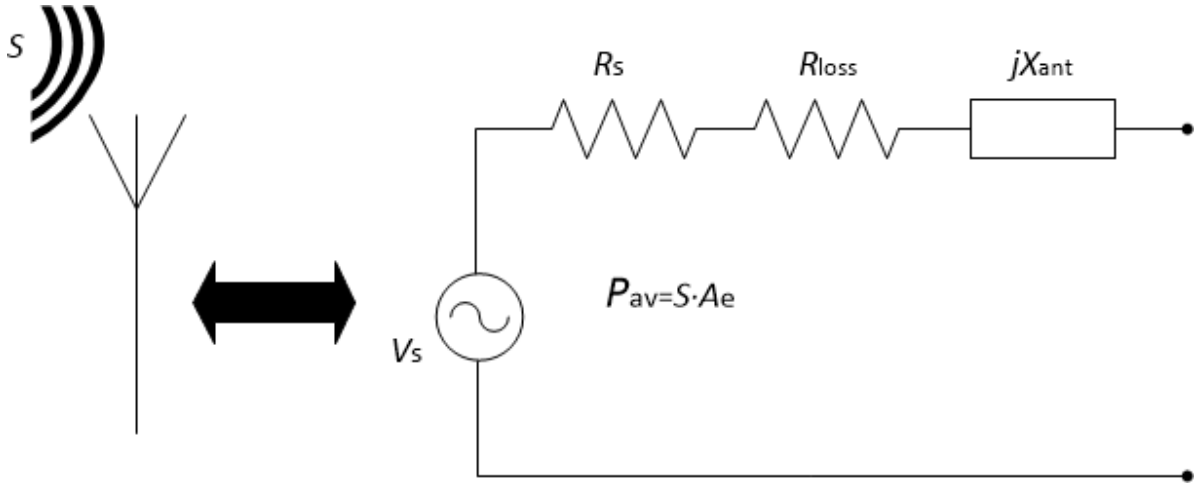

Fig. 1.3. Equivalent electrical model for an antenna

So, the impedance of the antenna (Z_{ant}) is $R_{\mathrm{s}} + jX_{\mathrm{ant}}$. The amplitude of the voltage generated on the antenna is given by: [1]

$$\hat{V}_{\mathrm{S}} = 2\sqrt{2R_{\mathrm{S}}P_{\mathrm{av}}} \tag{1.3}$$

Thus, $\hat{V}_{\mathrm{S}}$ increases for a larger R_{S} at a given P_{av}. In order to reduce the losses from the rectifier, due to dropping voltage, $\hat{V}_{\mathrm{S}}$ must be relatively high. P_{av} depends on A_{e} and S (see Fig. 1.3). In this way it depends on the antenna characteristics. Increasing A_{e}, by connecting several antennas (in series and/or in parallel) to form an array, produces an increase in P_{av}. However, this implies a larger physical area and, for some applications, it is not suitable. Efficiency depends on input power, and for microwatt level (about -10 dBm) is about 50 % [4][6]. First, in this project AC voltage source is used instead of antenna to simplify the prototype design. Then, a real antenna implementation was done.

1.2.2. Impedance matching

The maximum power transfer theorem, states that for DC circuits, the maximum power will be transferred from a source to its load if the load resistance is equal to the source resistance. In AC, the same theorem states that the maximum transfer of power, from a source to its load, occurs when the load impedance (Z_L) is equal to the complex conjugate of the source impedance (Z_S). Thus, if the source impedance is $Z_S = R_S + jX$, thus, its complex conjugate will be $Z_S^* = R_S - jX$. [2]

As an example, Fig. 1.4 shows a voltage source with an output impedance (Z_S) composed by R_S and a series reactive component of $+jX_S$ (an inductor) and a load impedance (Z_L) composed by R_L and a series reactance (capacitor) - jX_L. Typically, the Z_L value is given by the sensor and it is different from the Z_S. Then, a matching network stage has to be used in order to force a load impedance to "look like" the complex conjugate of the source impedance, so that maximum power may be transferred to the load. Note that, reactances have a frequency dependence, which means that perfect impedance circuit matching can occurs only at resonance frequency. At specific frequency (resonant frequency) X_L is equal to X_S and cancellation occurs. As the frequency is moved away the resonant frequency, the impedance matching becomes worse until impedance matching does not exists.

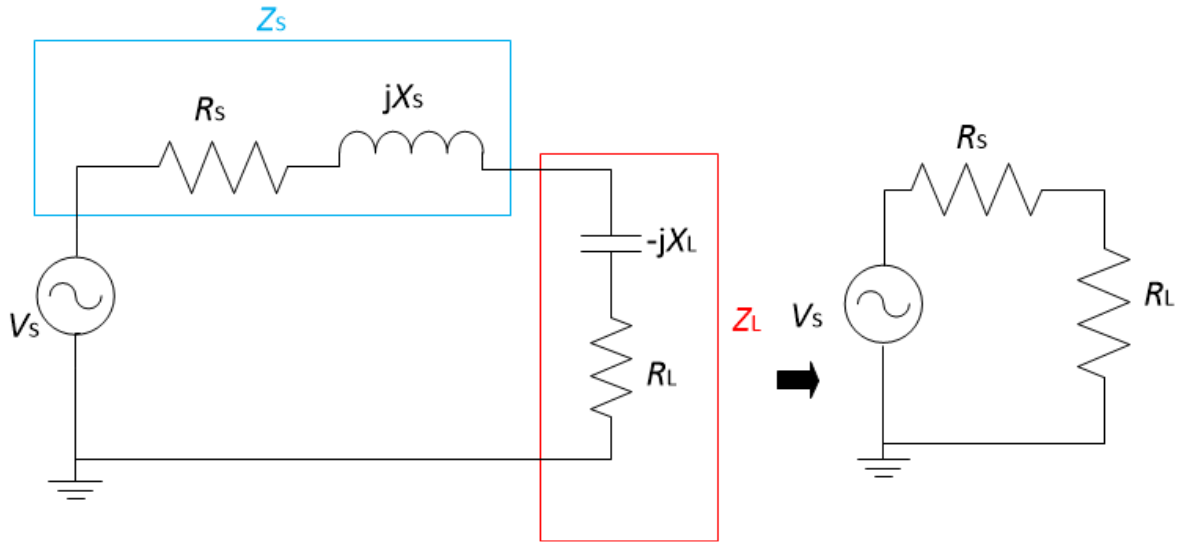

Fig. 1.4. Matching network scheme.

There are several numbers of possible networks that could be used to perform the impedance matching function. Three main circuits have been proposed for RF harvesting: a shunt-inductor (Fig. 1.5(a)), an L-network (Fig. 1.5(b)) and a transformer (Fig. 1.5(c)).

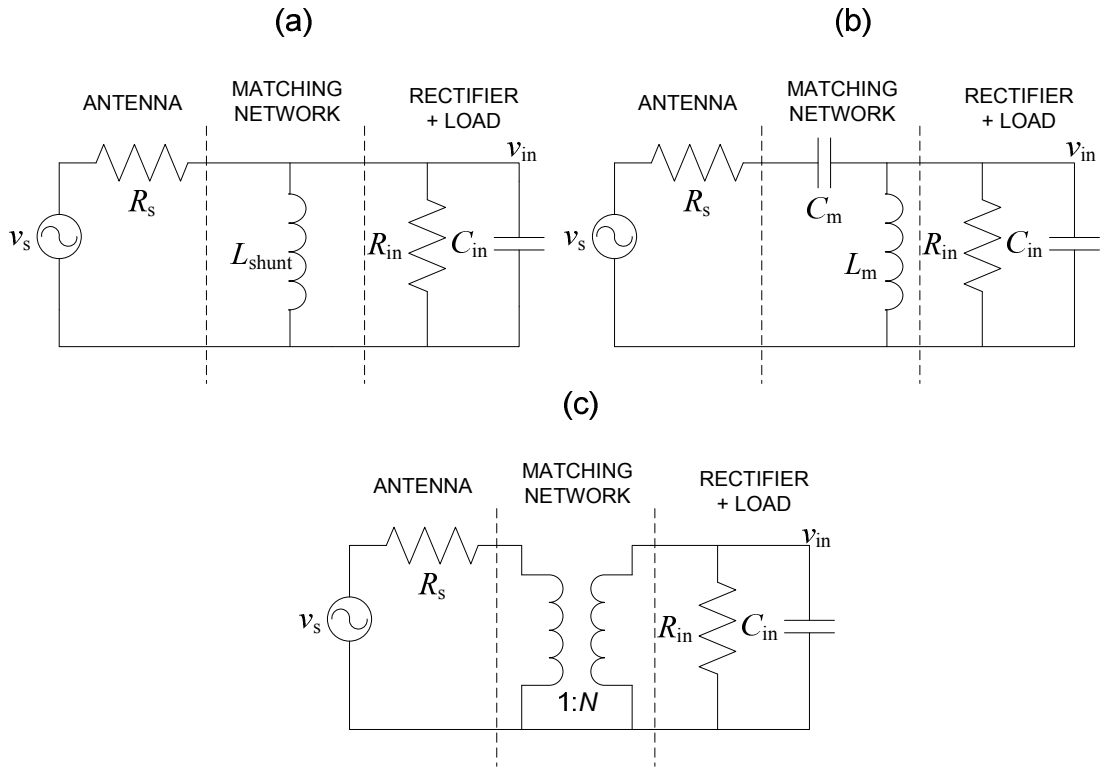

Fig. 1.5. Three different types of matching networks.

Whereby R_{in} and C_{in} are the equivalent impedance of both rectifier and load. A transformer used as matching network (Fig. 1.5(c)) can boosts the input voltage by the factor N, which is the ratio of the transformer's secondary voltage to its primary voltage. However, this solution it was not considered in this project.

The second matching network configuration is a shunt-inductor (Fig. 1.5(a)). L_{shunt} must resonate with $C_{\mathrm{in}}$of the rectifier in order to match the antenna and rectifier impedances. Therefore:

$$L_{\mathrm{shunt}} = \frac{1}{\omega_{\mathrm{r}}^2 \cdot C_{\mathrm{in}}} \tag{1.4}$$

Whereby ω_{r} is the angular resonant frequency. Thus, a high value of C_{in} requires a small value of L_{shunt}, which, in some cases, can be non-commercial. At the resonant

frequency, the input voltage at the rectifier (V_{in}) will come from the voltage divider between V_S, R_{S} and R_{in}. Obtaining the maximum power transfer when $R_{\mathrm{S}} = R_{\mathrm{in}}$. Thus, at low available power levels, V_{in} will be low and comparable with rectifier losses. Then, increasing the input voltage of the rectifier and reducing the losses of the rectifier will produces an increase of the efficiency. This is achieved by using high resistance antennas (a folded dipole has a radiation resistance of 300 Ω).

The ratio between the resonance frequency (f_{r}) and the circuit bandwidth at -3 dB (BW) is called quality factor (Q). For high *Q* values, BW is narrow. Therefore, the component's tolerance could produce a small deviation in f_{r} and a massive power drop at the rectifier input. So, a Q-BW trade-off should be taken into account. The circuit with the shunt-inductor matching network is an RLC parallel circuit with a resistance that is the parallel association of R_{S} and R_{in} ($R_{\mathrm{P}} = R_{\mathrm{S}}//R_{\mathrm{in}}$). Therefore:

$$Q = \frac{f_{\mathrm{r}}}{BW} = R_{\mathrm{P}} C_{\mathrm{in}} \omega_{\mathrm{r}} = \frac{R_{\mathrm{P}}}{\omega_{\mathrm{r}} L_{\mathrm{shunt}}} \tag{1.5}$$

Equation (1.5) shows that a high C_{in} (or low L_{shunt}) will result in a high *Q.* Thus, to obtain a reasonable BW, C_{in} must be kept low enough. Furthermore, a high value of R_{s} increases V_{S} which increases both V_{in} and *Q* but decreases BW.

The third configuration is L-network (Fig. 1.5(b)), which receives its name because of its component orientation, which resembles the shape of an L. Fig. 1.6 shows the four possible arrangements of the *L* and *C* components, one of which is already shown in Fig. 1.5(b). Two of the arrangements (Figs. 1.6-1 and 1.6-3) are in a low-pass configuration while the other two (Figs. 1.6-2 and 1.6-4) are in a high-pass configuration.

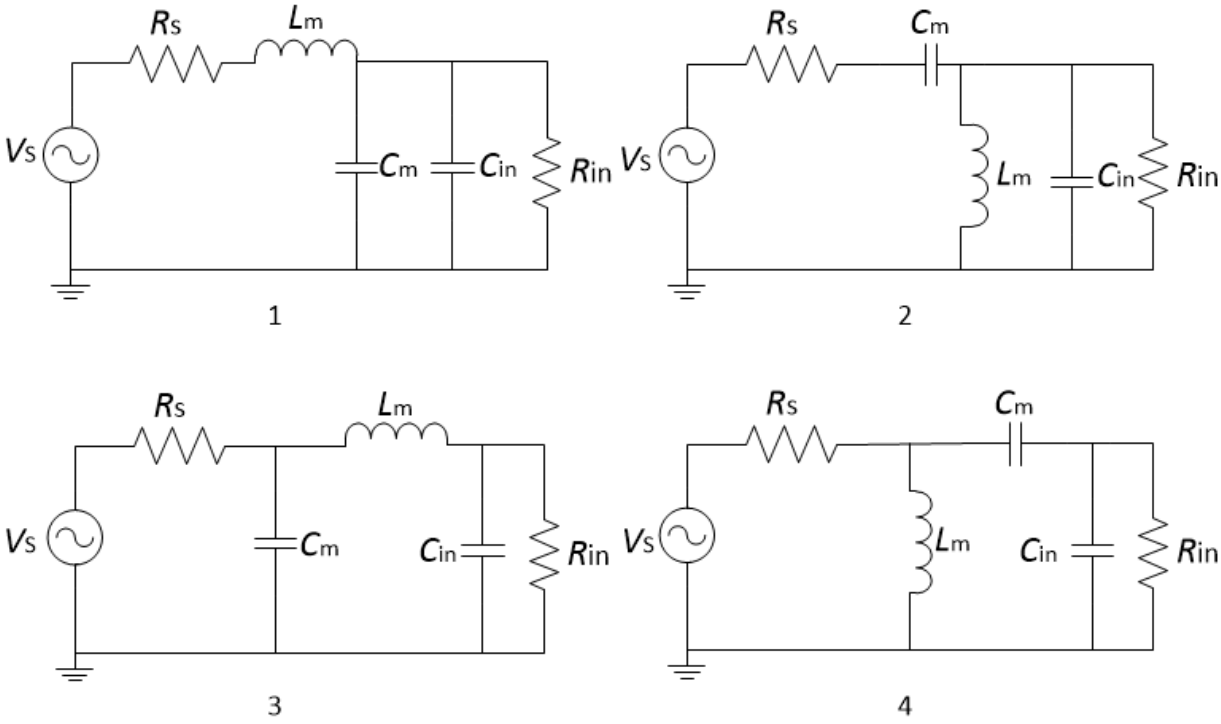

Fig. 1.6. Four types of L matching networks.

In some configurations an L-network can boost the antenna voltage (Fig. 1.6-1 and Fig. 1.6-2). This boost provides a higher peak voltage to the rectifier and thus offers comparatively better rectifier efficiency when P_{av} is low (and therefore V_{S}). To match the antenna with the load impedance and obtain a resonant circuit, the impedance at the input of the matching network must be the conjugate of the antenna impedance. Thus, equating the real and imaginary parts of both impedances generates two equations that enable calculation of the values of L_{m} and C_{m}. In this project the configuration of Fig. 1.6-1 and Fig. 1.6-2 could be used, since it allows the antenna voltage boost. However, the Fig. 1.6-2 has been arbitrarily chosen. Chapter 2 will show a detailed theoretical analysis of this configuration.

1.2.3. Rectifier

Circuits based on rectifiers provide a DC output voltage to the load. Three main options exist for the rectifier:

- A diode (together with the antenna becomes a rectenna) (Fig. 1.7(a));

- A bridge of diodes (or diode-connected transistors) (Fig. 1.7(b));

- A voltage rectifier multiplier (Fig. 1.8(a)).

All of the previous options have a broadband behaviour (i.e. they show the same rectifying characteristics in a broad band of frequencies). For kilohertz or megahertz frequencies, p-n diodes and transistors are used as rectifiers. On the other hand, for microwave frequencies, Schottky diodes (GaAs or Si type) are preferred, because of their shorter transit times. In addition, their forward voltage is lower which leads to a higher efficiency. The rectification performance of the diode depends on its saturation current, its junction capacitance and its conduction resistance. In order to lead to a low forward voltage drop, a large saturation current is looked for.

The diode (Fig. 1.7(a)) and the diode bridge (Fig. 1.7(b)) provide an output DC voltage to the load (V_{out}). This amplitude becomes lower than the peak voltage of the incoming signal.

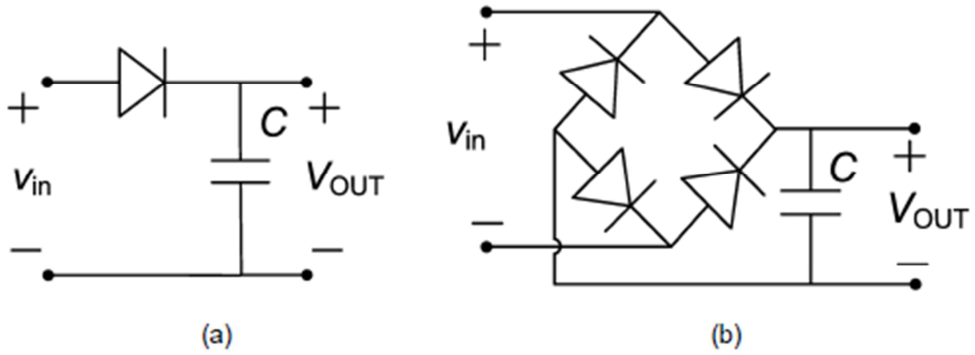

Fig. 1.7. Two kinds of rectifiers. [1]

The voltage rectifier multiplier (Fig. 1.8(a)) provides an output voltage that doubles the input voltage amplitude. An ideal diode (i.e. 0 V threshold voltage, no reverse current, and zero conduction resistance) is assumed and a sinusoidal wave is considered for V_{in}.

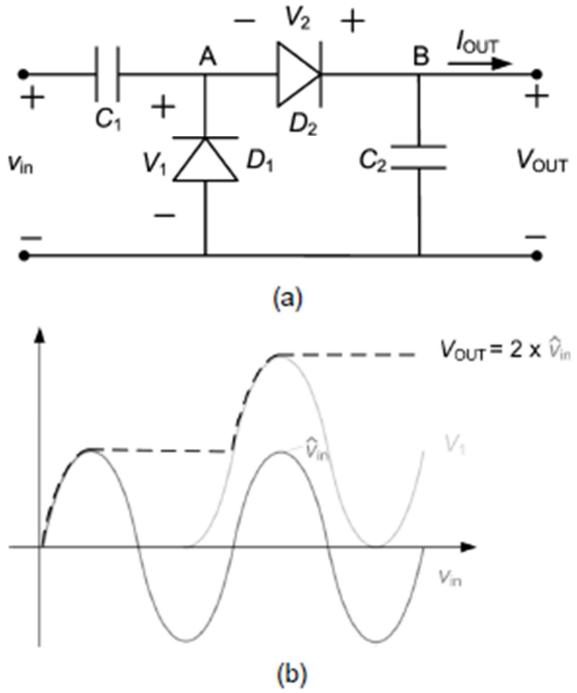

Fig. 1.8. Voltage rectifier multiplier. [1]

With reference to Fig. 1.8, a DC reference for the voltage at point A is established by diode D_1 and capacitor C_1. D_1 conducts if the voltage at point A is negative, and then builds an average charge at C_1that prevents the voltage at point A from ever going negative. Considering that all the elements are ideal, then the voltage at this point is $\hat{V}_{\text{in}}$+ V_{in} (V_1 in Fig. 1.8(b)). D_2 rectifies the signal at point A and capacitor C_2holds the output voltage (V_{out}) at the peak value of V_1. Thus, the open circuit voltage (OCV) of the rectifier is a DC voltage with a value $2\hat{V}_{\text{in}}$. In steady-state operation, I_{out} is drained from C_2, and this capacitor is recharged when V_1 is higher than V_{out} (dashed line in Fig. 1.8(b)). In order to obtain higher output voltages, the circuit can be cascaded by using N stages. In the case of an N-stage rectifier, V_{out} in open circuit is:

$$V_{\text{out}} = 2N\hat{V}_{\text{in}} \tag{1.6}$$

In a lossless rectifier, the input power (P_{in}) is equal to the output power (P_{out}) and an equivalent R_{in} can be calculated from the resistance connected at the output (R_{L}) as:

$$R_{\mathrm{in}} = \frac{V_{\mathrm{in}}^2}{2P_{\mathrm{in}}} = \frac{V_{\mathrm{out}}^2}{P_{\mathrm{out}}}\frac{1}{8N^2} = \frac{R_{\mathrm{L}}}{8N^2} \tag{1.7}$$

Thus, for a fixed R_{L}, as N increases, R_{in} decreases. Otherwise, for a matched value of $R_{\mathrm{in}} = R_{\mathrm{ant}}$, the optimum value of R_{L} increases as N increases.

When considering the dropping voltage of the diodes (V_{d}), the OCV is:

$$V_{\mathrm{out}} = 2N(\widehat{V}_{\mathrm{in}} - V_{\mathrm{d}}) \tag{1.8}$$

In a real world the rectifier has non-zero dropping voltage. Therefore, the output voltage will be lower than the input voltage at the rectifier (Fig. 1.8). Besides, the dropping voltage increases with the output current. Then, an approximate model by simplifying the behaviour of the rectifier is shown [17]:

$$P_{\mathrm{out}} = \frac{V_{\mathrm{out}}^2}{R_{\mathrm{L}}} = \frac{2N\left(\hat{V}_{in} - V_{\mathrm{d}}\right)^2}{R_{\mathrm{L}}} \tag{1.9}$$

From a DC point of view, the output current (I_{out}) flows from the input through the rectifier generating a power dissipation P_{loss}:

$$P_{\mathrm{loss}} = 2NV_{\mathrm{d}}I_{\mathrm{out}} = \frac{(2N)^2V_{\mathrm{d}}\left(\hat{V}_{in} - V_{\mathrm{d}}\right)}{R_{\mathrm{L}}} \tag{1.9}$$

Whereby the relationship $I_{\mathrm{out}} = V_{\mathrm{out}}/R_{\mathrm{L}}$ is used. Therefore:

$$P_{\mathrm{in}} = P_{\mathrm{out}} + P_{\mathrm{loss}} = \frac{(2N)^2V_{\mathrm{d}}\left(\hat{V}_{in}{}^2 - \hat{V}_{in}V_{\mathrm{d}}\right)}{R_{\mathrm{L}}} \tag{1.10}$$

Operating with (1.7):

$$R_{\mathrm{in}} = \alpha \frac{R_{\mathrm{L}}}{8N^2} \tag{1.11}$$

Being:

$$\alpha = \frac{1}{1 - \frac{V_{\mathrm{d}}}{\hat{V}_{in}}} \tag{1.12}$$

An accurate mathematical analysis of the real rectifier is quite complex. Simulations can be helpful to facilitate rectifier design. Furthermore, the whole system (antenna, matching network and rectifier) must be jointly analysed in order to obtain meaningful results [1].

On the other hand, R_{in} for a simple diode is found by assuming that all the input power at the rectifier is transferred to the load. Considering the power expressions for an AC and DC signal:

$$\begin{gathered} \frac{\hat{V}_{in}{}^2}{2R_{\mathrm{in}}} = \frac{V_{\mathrm{DC}}^2}{R_{\mathrm{L}}} \\ \hat{V}_{in} = V_{\mathrm{DC}} \\ 2R_{\mathrm{in}} = R_{\mathrm{L}} \rightarrow R_{\mathrm{in}} = \frac{R_{\mathrm{L}}}{2} \end{gathered} \tag{1.13}$$

Whereby V_{DC} is the voltage at the output of the rectifier. Whereas R_{in} is proportional to R_{L}.

1.3. Microstrip transmission lines

As will be shown in Chapter 4, a PCB implementation of the energy harvesting system with a working frequency of 868 MHz will be performed. So, it is important to take into account some basic concepts of transmission lines. In this section a short review of microstrip transmission lines is done.

A microstrip is a type of electrical transmission line which can be fabricated using PCB technology. Microstrip lines are used to transmit microwave-frequency signals. They

consist of a conducting strip separated from a ground plane by a dielectric layer known as the substrate. Microwave components such as antennas, couplers, filters, power dividers, etc. can be formed from microstrip technology. It is much less expensive than traditional waveguide technology, as well as being far lighter and more compact.

For lowest cost, microstrip devices may be built on an ordinary FR-4 (standard PCB) substrate. However it is often found that the dielectric losses in FR4 are too high at microwave frequencies, and that the dielectric constant is not enough controlled. Even so, in this project FR-4 substrate was used.

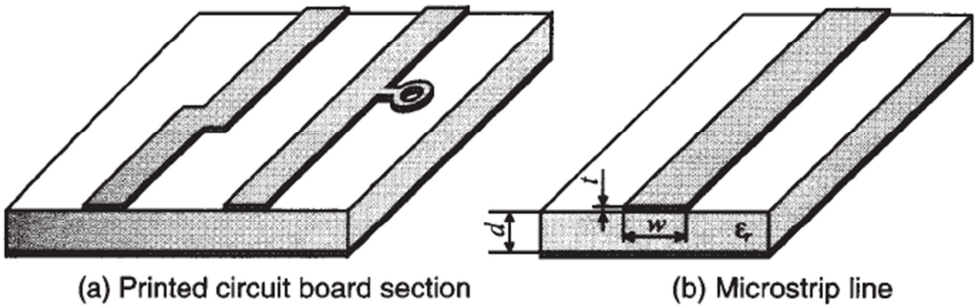

Fig. 1.9. Microstrip transmission line [2].

1.3.1. Inhomogeneity

The electromagnetic wave transported by a microstrip line exists in two parts: partly in the dielectric substrate and partly in the air above it. In general, the dielectric constant of the substrate will be different (and higher) than that of the air, so that the wave is travelling in a heterogeneous medium. In consequence, the propagation velocity is somewhere between the speed of radio waves in the substrate, and the speed of radio waves in air.

Consequences of an inhomogeneous medium are:

- The line is dispersive. With increasing frequency, the effective dielectric constant gradually changes towards that of the substrate, so that the phase velocity gradually decreases.

- The characteristic impedance of the line changes slightly with frequency (again, even with a non-dispersive substrate material).

- The wave impedance varies over the cross-section of the line.

1.3.2. Characteristic impedance

In this section the characteristic impedance ($Z_{\text{microstrip}}$) of microstrip line is calculated.

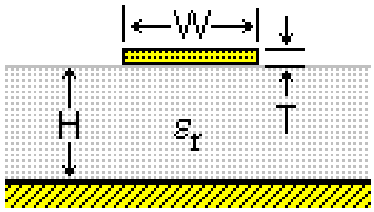

Fig. 1.10. Microstrip transmission line section. From TX- LINE® (National Instruments).

With reference to Fig. 1.10, a closed-form approximate expression for the quasi-static characteristic impedance of a microstrip line was developed by Wheeler [8]:

$$Z_{\text{microstrip}} = \frac{Z_0}{2\pi\sqrt{2(1+\varepsilon_r)}} \ln\left(1 + \frac{4h}{w_{\text{eff}}}\left(\frac{14+\frac{8}{\varepsilon_r}}{11}\frac{4h}{w_{\text{eff}}} + \sqrt{\left(\frac{14+\frac{8}{\varepsilon_r}}{11}\frac{4h}{w_{\text{eff}}}\right)^2 + \pi^2\frac{1+\frac{1}{\varepsilon_r}}{2}}\right)\right), \tag{1.14}$$

Where Z_0 is the impedance of free space, $\mathcal{E}_{\text{r}}$ is the relative permittivity of substrate, h is the thickness ("height") of substrate, and w_{eff} is the effective width of the strip, being:

$$w_{\text{eff}} = w + t\frac{1+\frac{1}{\varepsilon_r}}{2\pi}\ln\left(\frac{4e}{\sqrt{\left(\frac{t}{h}\right)^2 + \left(\frac{1}{\pi}\frac{1}{\frac{w}{t}+\frac{11}{10}}\right)^2}}\right). \tag{1.15}$$

Where w is the width of the strip and t is the thickness of the strip metallization.

This formula is asymptotic to an exact solution in three different cases:

1. $w \gg h$,, any $\mathcal{E}_{\text{r}}$ (parallel plate transmission line).
2. $w \ll h$, $\mathcal{E}_{\text{r}} = 1$ (wire above a ground-plane).
3. $w \ll h$, $\mathcal{E}_{\text{r}} \gg 1$.

Note that, the characteristic impedance of the microstrip line does not depend of the line length whenever the line is connected to an impedance equal than the characteristic line impedance. On the other hand, the transmission line can be connected to an impedance which value is different to the characteristic impedance of the line:

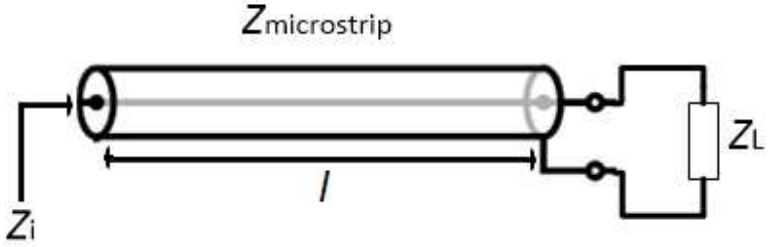

Fig. 1.11. Microstrip transmission line impedance.

Whereby Z_{i} is the equivalent input impedance of transmission line. Based on Fig. 1.11. Z_{i} of a low losses transmission line can be expressed as:

$$Z_{\mathrm{i}} = Z_0 \frac{Z_{\mathrm{L}} \cos \beta l + j Z_0 sin\beta l}{Z_0 \cos \beta l + j Z_{\mathrm{L}} sin\beta l} \tag{1.16}$$

Whereby l is the total lenght of the line and β is the phase constant. Two cases are studied for Z_{i} impedance:

1) Input impedance of a transmission line terminated in short circuit ($Z_{\mathrm{L}} = 0$).

$$Z_{\mathrm{i}} = Z_{\mathrm{sc}} = j\, Z_0 \tan \beta l \tag{1.17}$$

Whereby Z_{sc} is the equivalent short circuit impedance. A transmission line which is terminated in short circuit and placed in parallel to the circuit behaves as an inductance. The required transmission line length is founded by substituting the impedance value (Z_{sc}) at the expression (1.17):

$$l = \frac{1}{\beta} \mathrm{atan}\left(\frac{Z_{\mathrm{sc}}}{j\, Z_0}\right) \tag{1.18}$$

Whereby:

$$Z_{\mathrm{sc}} = j\omega \mathrm{L} \tag{1.19}$$

Being *L* the nominal value of the inductance.

2) Input impedance of a transmission line terminated in open circuit ($Z_{\mathrm{L}} \to \infty$).

$$Z_{\mathrm{i}} = Z_{\mathrm{oc}} = j\, Z_0 \cot \beta l \tag{1.20}$$

Whereby Z_{oc} is the equivalent open circuit impedance. A transmission line which is terminated in open circuit and placed in parallel to the circuit behaves as a capacitor. The required transmission line length is founded by substituting the impedance value (Z_{oc}) at the expression (1.20):

$$l = \frac{1}{\beta} \mathrm{atan}\left(\frac{j\, Z_0}{Z_{\mathrm{oc}}}\right) \tag{1.21}$$

Whereby:

$$Z_{\mathrm{oc}} = 1/j\omega \mathrm{C} \tag{1.22}$$

Being *C* the nominal value of the capacitance. The process of making a reactance with a transmission line is called stub.

CHAPTER 2. THEORETICAL ANALYSIS

In this chapter the matching network stage is theoretically analyzed and faced as crucial element in order to achieve a high efficiency. Efficiency is defined as the ratio between the delivered power to the load and the available power (P_{av}). So, the concept of efficiency establishes how much power is harnessed from the available input power. Usually the available ambient RF power is in the level of microwatts or below, so taking profit of the most available power will be a must. According with previous works [4], [5] the lower the available input power the lower the efficiency. However, in this thesis we will show, that with a properly choice of the matching network the efficiency for low input powers can be comparable to that with high input power conditions. This is achieved evaluating the rectifier as the critical element. A conventional rectifier includes a dropping voltage across the diodes that decrease the efficiency. The dropping voltage of Schottky diodes (for example 0,15 V for HSMS2850 model from Avago) could not seem critical at first. But for, $P_{\mathrm{av}} = -10\ dBm$ with a 50 Ω antenna impedance, for example, $\hat{V}_{\mathrm{s}} = 0.2\ V$ (according to (1.3)), which is comparable to the diode dropping voltage. So, a very low efficiency from the rectifier would be expected. For this reason, a passive amplification stage before the rectifier is required in order to not waste energy in an active amplifier. In this project the proposed solution is based on amplifying the voltage at the impedance matching stage. In this way, the dropping voltage across the rectifier compared to its input voltage will become less notorious. The L-network is a suitable configuration because it allows boosting the input voltage. The whole proposed circuit with an L-network is displayed in Fig. 2.1. However, when the input power is relatively high (around 10 dBm and above), a shunt-inductor matching network could be used because no amplification is needed.

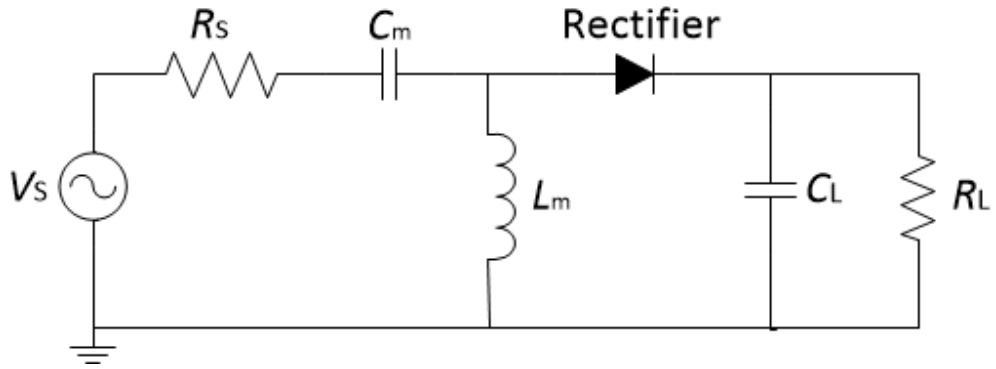

Fig. 2.1.Proposed circuit with an L-network.

With respect to Fig. 2.1, the antenna is roughly modelled as an AC voltage source (V_s) with a series impedance. The series impedance basically comprises a radiation resistance (R_s), a loss resistance and a reactive part. Here, the loss resistance and reactive part are neglected.

$C_m$and L_m are the passive matching network elements that will be in charge of boosting the input voltage of the rectifier.

A rectifier based on a Schottky diode is chosen because of its low dropping voltage. Regarding to the load, a resistance (R_L) could simulate an autonomous sensor. A variable resistor will be used in order to track the maximum efficiency point as a function of the load resistance. The capacitor C_L has a relative high value and holds the output voltage constant.

2.1. L-network matching network

A detailed theoretical analysis for an L-network setup is provided here. The formulation has to be developed to describe all the parameters involved in the boost voltage process. Fig. 2.2 is a simplified schematic circuit of Fig. 2.1 where R_{in} and C_{in} are the equivalent impedance of both, the rectifier and the load.

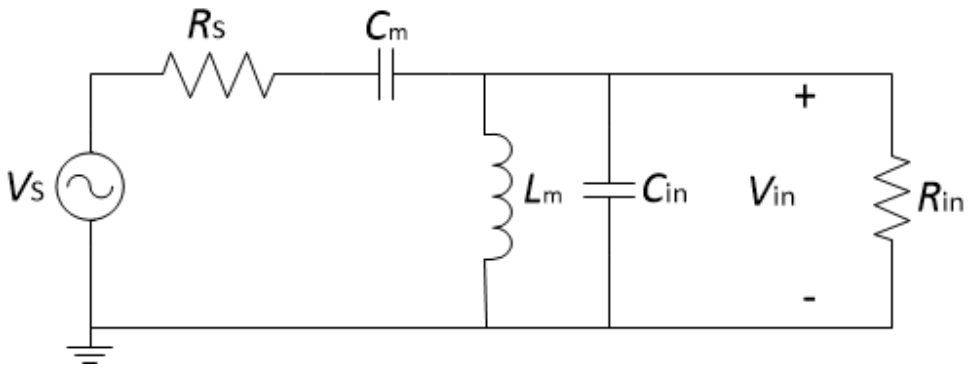

Fig. 2.2. L-network scheme.

First of all the main aim of the L-network is matching the antenna with the load impedance. Exhaustive theoretical analysis and the formulation obtaining must be performed before the C_m and L_m values definition. Then, the first step is the goal definition:

$$R_S = Z_{eq} \tag{2.1}$$

Whereby Z_{eq} is the equivalent impedance. To match the load with the antenna impedance, the reactive part removal must be done. This is done by splitting the L_m in two inductances: L'_m is intended to eliminate the C_{in} capacitance and L''_m tries to resonate with C_m capacitance.

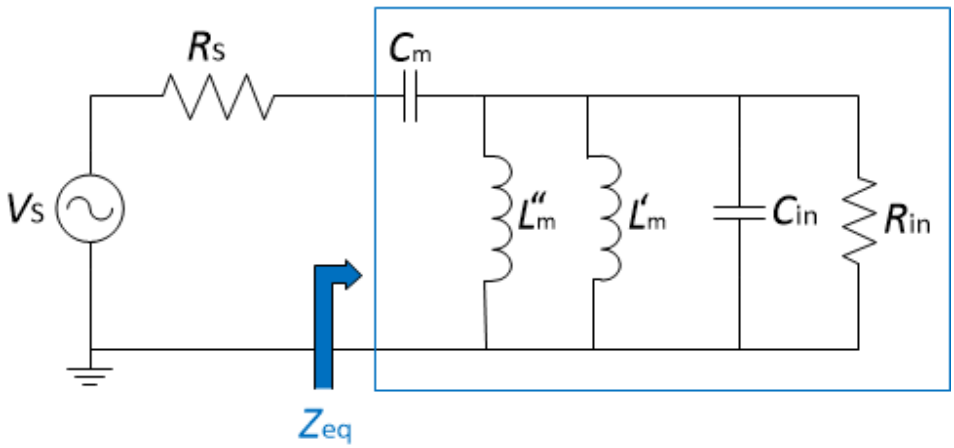

Fig. 2.3. Two inductances L_m to match the circuit.

Now L'_m is matched with C_{in} following the next condition:

$$Y = \frac{-j}{\omega L'_m} + j\omega C_{in} = 0$$

$$j\omega C_{in} = \frac{j}{\omega L'_m} \rightarrow \omega^2 = \frac{1}{L'_m C_{in}} \tag{2.2}$$

Whereby :

$$\omega = 2\pi f \tag{2.3}$$

Whereby $f = f_r$ is the ISM band frequency of the system (868 MHz). Finally, the L'_m expression is obtained:

$$L'_{\mathrm{m}} = \frac{1}{\omega^2 C_{\mathrm{in}}} \tag{2.4}$$

Once L'_{m} is compensated with C_{in}, the equivalent circuit is:

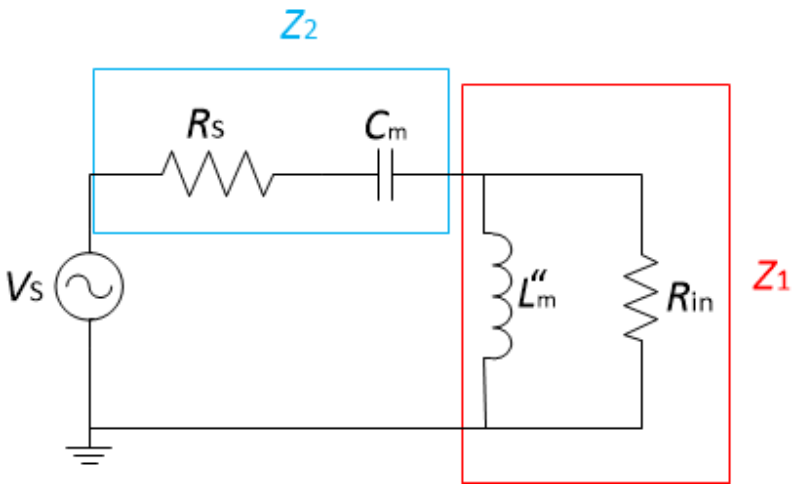

Fig. 2.4. Impedances matching.

Whereby:

$$Z_1 = R_{\mathrm{in}} // j\omega L''_{\mathrm{m}} \tag{2.5}$$

$$Z_2 = R_{\mathrm{s}} + \frac{-j}{\omega C_{\mathrm{m}}} \tag{2.6}$$

The real and imaginary part of both impedances has to be matched:

$$\begin{aligned} Re\{Z_1\} &= Re\{Z_2\} \\ Im\{Z_1\} &= Im^*\{Z_2\} \end{aligned} \tag{2.7}$$

Note that, the Z_2 impedance is the sum between R_s and C_m because the two elements are in series. On the other hand, Z_1 must be calculated:

$$Z_1 = \frac{R_\mathrm{in} \cdot j\omega L''_\mathrm{m}}{R_\mathrm{in} + j\omega L''_\mathrm{m}} = \frac{R_\mathrm{in} \cdot j\omega L''_\mathrm{m} \cdot (R_\mathrm{in} - j\omega L''_\mathrm{m})}{(R_\mathrm{in} + j\omega L_\mathrm{m}) \cdot (R_\mathrm{in} - j\omega L_\mathrm{m})} = \frac{R_\mathrm{in}^2 \cdot j\omega L''_\mathrm{m} + R_\mathrm{in}\omega^2 (L''_\mathrm{m})^2}{R_\mathrm{in}^2 + \omega^2 (L''_\mathrm{m})^2} \tag{2.8}$$

$$Re\{Z_1\} = \frac{R_\mathrm{in}\omega^2 (L''_\mathrm{m})^2}{R_\mathrm{in}^2 + \omega^2 (L''_\mathrm{m})^2} \tag{2.9}$$

$$Im\{Z_1\} = \frac{jR_\mathrm{in}^2 \omega L''_\mathrm{m}}{R_\mathrm{in}^2 + \omega^2 (L''_\mathrm{m})^2} \tag{2.10}$$

Once the real (2.9) and imaginary (2.10) part of Z_1 are found, then Z_1 has to be matched with Z_2:

$$\begin{aligned} R_\mathrm{s} &= \frac{R_\mathrm{in}\omega^2 L_\mathrm{m}^2}{R_\mathrm{in}^2 + \omega^2 L_\mathrm{m}^2} \\ \frac{-j}{\omega C_\mathrm{m}} &= \frac{jR_\mathrm{in}^2 \omega L''_\mathrm{m}}{R_{in}^2 + \omega^2 L_\mathrm{m}^2} \end{aligned} \tag{2.11}$$

From the real part of (2.11) expression, L''_m is found:

$$\begin{aligned} R_\mathrm{in}^2 R_\mathrm{s} + \omega^2 (L''_\mathrm{m})^2 R_\mathrm{s} = R_\mathrm{in}\omega^2 (L''_\mathrm{m})^2 &\rightarrow (L''_\mathrm{m})^2 (R_\mathrm{in}\omega^2 - \omega^2 R_\mathrm{s}) = R_\mathrm{in}^2 R_\mathrm{s} \\ R_\mathrm{in}\omega \cdot \sqrt{\frac{R_\mathrm{s}}{R_\mathrm{in} - R_\mathrm{s}}} L''_\mathrm{m} &= \frac{1}{\omega} \sqrt{\frac{R_\mathrm{in}^2 R_\mathrm{s}}{R_\mathrm{in} - R_\mathrm{s}}} \\ L''_\mathrm{m} &= \frac{R_\mathrm{in}}{\omega} \sqrt{\frac{R_\mathrm{S}}{R_\mathrm{in} - R_\mathrm{s}}} \end{aligned} \tag{2.12}$$

After L''_{m} is found, the L_{m} must be calculated following the next expression:

$$\frac{1}{L_{\mathrm{m}}} = \frac{1}{L''_{\mathrm{m}}} + \frac{1}{L'_{\mathrm{m}}} \tag{2.13}$$

Operating:

$$\frac{1}{L_{\mathrm{m}}} = \frac{1}{\frac{R_{\mathrm{in}}}{\omega}\sqrt{\frac{R_{\mathrm{S}}}{R_{\mathrm{in}} - R_{\mathrm{S}}}}} + \frac{1}{\frac{1}{\omega^2 \cdot C_{\mathrm{in}}}} = \frac{1}{\frac{R_{\mathrm{in}}}{\omega}\sqrt{\frac{R_{\mathrm{S}}}{R_{\mathrm{in}} - R_{S}}}} + \omega^2 \cdot C_{\mathrm{in}} =$$

$$= \frac{\frac{R_{\mathrm{in}}}{\omega}\omega^2 \cdot C_{\mathrm{in}}\sqrt{\frac{R_{\mathrm{S}}}{R_{\mathrm{in}} - R_{\mathrm{S}}}} + 1}{\frac{R_{\mathrm{in}}}{\omega}\sqrt{\frac{R_{\mathrm{S}}}{R_{\mathrm{in}} - R_{\mathrm{s}}}}} = \frac{R_{\mathrm{in}}\omega \cdot C_{\mathrm{in}}\sqrt{\frac{R_{\mathrm{S}}}{R_{\mathrm{in}} - R_{\mathrm{S}}}} + 1}{\frac{R_{\mathrm{in}}}{\omega}\sqrt{\frac{R_{\mathrm{S}}}{R_{\mathrm{in}} - R_{\mathrm{s}}}}}$$

$$= \frac{\frac{R_{\mathrm{in}}}{w}\sqrt{\frac{R_{S}}{R_{\mathrm{in}} - R_{S}}}}{R_{\mathrm{in}}\omega \cdot C_{\mathrm{in}}\sqrt{\frac{R_{\mathrm{S}}}{R_{\mathrm{in}} - R_{\mathrm{S}}}} + 1}$$

$$L_{\mathrm{m}} = \frac{R_{\mathrm{in}}}{\omega}\frac{1}{R_{\mathrm{in}}\omega \cdot C_{\mathrm{in}} + \frac{1}{\sqrt{\frac{R_{\mathrm{S}}}{R_{\mathrm{in}} - R_{\mathrm{S}}}}}} \tag{2.14}$$

From the imaginary part of (2.11) expression, C_{m} is found introducing the L_{m} expression:

$$\frac{1}{C_{\mathrm{m}}} = \frac{R_{\mathrm{S}}^2\omega\cdot(\frac{R_{\mathrm{in}}}{\omega}\cdot\sqrt{\frac{R_{\mathrm{S}}}{R_{\mathrm{in}}-R_{\mathrm{S}}}})}{R_{\mathrm{in}}^2+\omega^2\frac{R_{\mathrm{in}}^2}{\omega^2}\cdot(\cdot\sqrt{\frac{R_{\mathrm{S}}}{R_{\mathrm{in}}-R_{\mathrm{S}}}})^2} \rightarrow \frac{1}{C_{\mathrm{m}}} = \frac{R_{\mathrm{S}}^3\omega\cdot\sqrt{\frac{R_{\mathrm{S}}}{R_{\mathrm{in}}-R_{\mathrm{S}}}}}{R_{\mathrm{in}}^2+\frac{R_{in}^2R_{\mathrm{S}}}{R_{\mathrm{in}}-R_{S}}} \rightarrow \frac{1}{C_{\mathrm{m}}} = \frac{R_{\mathrm{S}}\omega\cdot\sqrt{\frac{R_{\mathrm{S}}}{R_{\mathrm{in}}-R_{\mathrm{S}}}}}{1+\frac{R_{\mathrm{S}}}{R_{\mathrm{in}}-R_{\mathrm{S}}}} \rightarrow$$

$$\frac{1+\frac{R_{\mathrm{S}}}{R_{\mathrm{in}}-R_{\mathrm{S}}}}{C_{\mathrm{m}}} = R_{\mathrm{s}}\omega\cdot\sqrt{\frac{R_{\mathrm{S}}}{R_{\mathrm{in}}-R_{\mathrm{S}}}} \rightarrow C_{\mathrm{m}} = \frac{1+\frac{R_{\mathrm{S}}}{R_{\mathrm{in}}-R_{\mathrm{S}}}}{R_{\mathrm{S}}\omega\cdot\sqrt{\frac{R_{\mathrm{S}}}{R_{\mathrm{in}}-R_{\mathrm{S}}}}} \rightarrow$$

$$C_{\mathrm{m}} = \frac{\sqrt{\frac{R_{\mathrm{s}}}{R_{\mathrm{in}} - R_{\mathrm{s}}}} + \frac{R_{\mathrm{s}}}{R_{\mathrm{in}} - R_{\mathrm{s}}} \cdot \sqrt{\frac{R_{\mathrm{s}}}{R_{\mathrm{in}} - R_{\mathrm{s}}}}}{R_{\mathrm{s}}\omega \cdot \sqrt{\frac{R_{\mathrm{s}}}{R_{\mathrm{in}} - R_{\mathrm{s}}}}}$$

$$C_{\mathrm{m}} = \frac{1}{R_{\mathrm{s}} w} \sqrt{\frac{R_{\mathrm{s}}}{R_{\mathrm{in}} - R_{\mathrm{s}}}} \tag{2.15}$$

After L_{m} and C_{m} expression have been obtained, the quality factor (*Q*) expression has to be calculated. This factor gives the relationship between the bandwidth of the system and its resonant frequency.

$$Q = \frac{f_{\mathrm{c}}}{\mathrm{BW}} \tag{2.16}$$

To achieve the *Q* expression system, a reformulation of the problem in terms of admittances is proposed. In this way, the source and load admittances must be matched:

$$Y_{\mathrm{s}}^{*} = Y_{\mathrm{L}} = G_{\mathrm{in}} + j(\omega C_{\mathrm{in}} - \frac{1}{\omega L_{\mathrm{m}}}) \tag{2.17}$$

Whereby Y_{s} and Y_{L} are the source and load admittances respectively. Transforming to conductances:

$$G_{\mathrm{in}} = \frac{\omega^2 C_{\mathrm{m}}^2 R_{\mathrm{s}}}{1+\omega^2 C_{\mathrm{m}}^2 R_{\mathrm{s}}^2} \rightarrow R_{\mathrm{in}} = \frac{1+\omega^2 C_{\mathrm{m}}^2 R_{\mathrm{s}}^2}{\omega^2 C_{\mathrm{m}}^2 R_{\mathrm{s}}} \tag{2.18}$$

Whereby G_{in} is the input conductance of the system. Taking into account the source Q_{s} expression:

$$Q_{\mathrm{s}} = \frac{1}{\omega C_{\mathrm{m}} R_{\mathrm{S}}} \tag{2.19}$$

Working with $R_s$and Q:

$$R_{in} = \frac{1 + \omega^2 C_m^2 R_S^2}{\omega^2 C_m^2 R_S^2} R_S = R_S(1 + \frac{1}{(\omega C_m R_s)^2}) = R_s(1 + {Q_s}^2) \quad (2.20)$$

The final system Q expression only with resistances dependence is:

$$Q = \sqrt{\frac{R_{in}}{R_S} - 1} \quad (2.21)$$

Another important parameter which expression must be obtained is the transfer function. Since, it allows determining the desired value. The first step to easily get this expression is converting the circuit to a series circuit. The new series circuit is shown below:

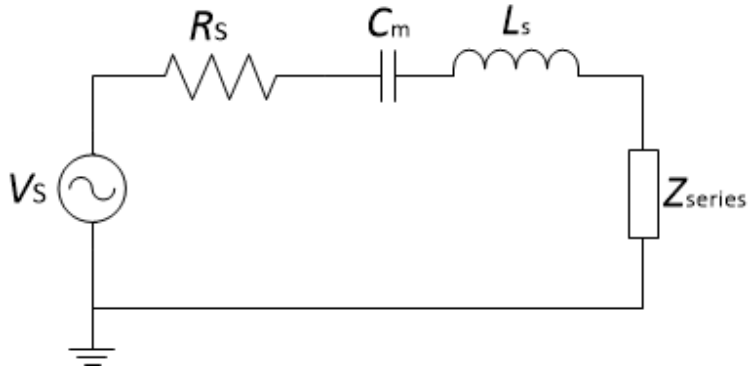

Fig. 2.5. Equivalent series circuit.

Whereby Z_{series} is the equivalent series impedance of the load. As can be appreciated, a new item L_s appears. Where:

$$L_S = \frac{1}{\omega^2 C_m} \quad (2.22)$$

To find the transfer function, the series circuit current definition must be done:

$$I = \frac{V_S}{2R_S} \rightarrow V_{in} = I \cdot (R_S + j\omega L_S) \tag{2.23}$$

With the *I* definition and V_{in}, the transfer function is obtained by applying the V_{in} and V_S relation:

$$H(\omega) = \frac{V_{in}}{V_s} \tag{2.24}$$

Taking the expression of the V_{in}:

$$V_{in} = \frac{V_S}{2R_S}(R_S + j\omega L_S) \rightarrow |V_{in}| = \frac{V_S \cdot \sqrt{R_S^2 + (\omega L_s)^2}}{2R_s} = \frac{V_S}{2} \cdot \sqrt{\frac{R_S^2 + (\omega L_s)^2}{R_S^2}} =$$

$$= \frac{V_S}{2} \cdot \sqrt{1 + (\frac{wL_s}{R_S})^2} \tag{2.25}$$

If the *Q* expression is taken:

$$Q_S = Q_L = \frac{\omega L_S}{R_S} = \frac{1}{\omega C_m R_S} = Q \tag{2.26}$$

Then:

$$\frac{V_S}{2}\sqrt{1 + Q^2} \rightarrow \frac{V_{in}}{V_S} = H = \frac{1}{2} \cdot \sqrt{1 + Q^2} \rightarrow H = \frac{1}{2} \cdot \sqrt{\frac{R_{in}}{R_S}} \tag{2.27}$$

Whereby H is the transfer function which shows that a gain (G) appears when the R_{in} is higher than R_S. This is an important feature of the system because it allows setting a desired gain by playing with the load.

2.2. Practical design procedure

This section wants to explain how is the theoretical process to match the circuit impedances by using the formulation described in section 2.1.

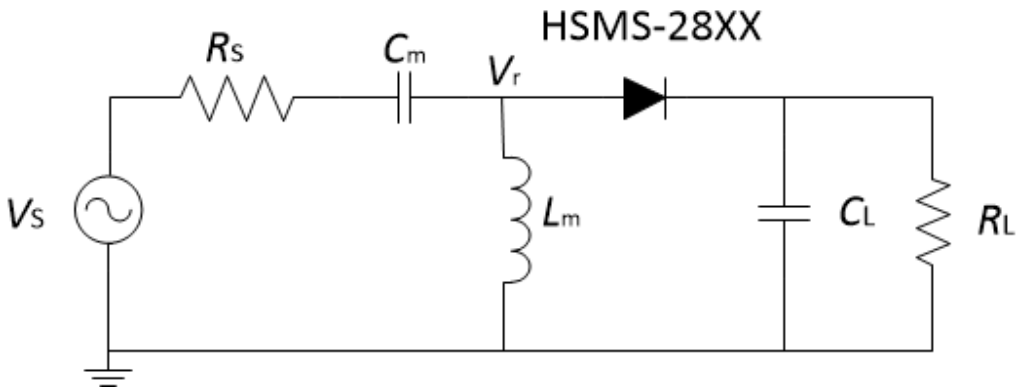

Fig. 2.6. Parameters in circuit schematic

Note that, V_{r} is not a parameter provided by the system. Considering the dropping voltage of the rectifier and the quality factor, a value for V_{r} is proposed in order to make V_{d} criticalless and able to maintain the *Q* not too high (then, an acceptable bandwidth is gotten). So, ideally, the dropping voltage would be the only factor that causes losses. In the next chapter, the simulations will show that this supposition is not true. First, the V_d impact is checked:

$$L_{\mathrm{eff}}(\%) = \frac{V_{\mathrm{d}}}{V_{\mathrm{r}}} \cdot 100 \tag{2.28}$$

Whereby L_{eff} are the efficiency losses due to the dropping voltage of the rectifier. Q expression:

$$Q = \sqrt{\frac{R_{\mathrm{in}}}{R_{\mathrm{S}}} - 1} \tag{2.29}$$

R_{in} must be calculated. From the gain expression it is gotten:

$$G = \frac{V_r}{V_s} = \frac{1}{2} \cdot \sqrt{\frac{R_{in}}{R_s}} \tag{2.30}$$

V_s is obtained directly from (1.3). Now it is possible to obtain firstly the gain, secondly R_{in} and then Q:

$$G = \frac{V_r}{V_s} \tag{2.31}$$

$$G = \frac{1}{2} \cdot \sqrt{\frac{R_{in}}{R_s}} \rightarrow R_{in} \tag{2.32}$$

$$Q = \sqrt{\frac{R_{in}}{R_S} - 1} \tag{2.33}$$

Having Q, the bandwidth is obtained:

$$Q = \frac{f}{BW} \rightarrow BW \tag{2.34}$$

As an example, a set of mandatory parameters are chosen in order to show how the process has been done in this project.

Acronym	Value	Magnitude
P_{av}	-10 dBm	Available power collected by the antenna
R_s	50 Ω	Antenna series resistance
C_R	0.18 pF	Input equivalent HSMS2850 rectifier capacitance
V_d	0.15 V	Dropping voltage of HSMS2850 rectifier
V_r	1 V	Input rectifier voltage
f	868 MHz	Operating (resonance) frequency

Fig. 2.7. Predefined system values.

A commercial rectifier (HSMS-2850 from Avago) based on Schottky diode is chosen because of its low dropping voltage. This rectifier will allow having low source voltage and so, working better at low input powers. After the verifications and considering Fig. 2.7., the variables values are:

Variable	Value
$\boldsymbol{L_{\mathrm{eff}}(\%)}$	15
$\boldsymbol{G}$	5
$\boldsymbol{R_{\mathrm{in}}(\Omega)}$	5000
$\boldsymbol{Q}$	9.95
$\mathbf{BW(MHz)}$	87.23

Fig. 2.8. Matching parameters

The values obtained in Fig. 2.8. allow finding the components of the matching L-network by applying (2.14) and (2.15):

$$C_{\mathrm{m}} = 368\ fF \tag{2.35}$$

$$L_{\mathrm{m}} = 61.7\ nH \tag{2.36}$$

CHAPTER 3. CIRCUIT ANALYSIS AND SIMULATIONS

After the theoretical analysis, a step before the prototype implementation is required. This step is related with the circuit analysis and simulations. Two matching network setups are compared and simulated. Simulations are useful to create an approximation of the results that will be obtained with the real PCB implementation. The simulations will be carried out with Advanced Design System (ADS) from Agilent Technologies.

3.1. Definition of elements in ADS simulations

The elements used in ADS simulations will be defined in this section in order to understand the way that the results are shown.

3.1.1. Lumped components

The lumped element model (also called lumped parameter model, or lumped component model) simplifies the description of the behaviour of spatially distributed physical systems into a topology consisting of discrete entities that approximate the behaviour of the distributed system under certain assumptions. It is useful in electrical systems (including electronics), mechanical multibody systems, heat transfer, acoustics, etc.

Mathematically speaking, the simplification reduces the state space of the system to a finite number, and the partial differential equations (PDEs) of the continuous (infinite-dimensional) time and space model of the physical system into ordinary differential equations (ODEs) with a finite number of parameters.

3.1.2. VtSine (Voltage Source, Decaying Sine Wave)

VtSine is the voltage source used to simulate the antenna.

3.1.2.1. Symbol

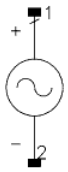

Fig. 3.1. ADS VtSine symbol

3.1.2.2. Parameters

Name	Description	Units	Default
V_{dc}	Initial voltage offset	V	0
Amplitude	Amplitude of sinusoidal wave	V	1
Freq	Frequency of sinusoidal wave	GHz	1
Delay	Time delay	ns	0
Damping	Damping factor	None	0
Phase	Phase value	deg	0
SaveCurrent	Flag to save branch current: yes, no	None	no

Fig. 3.2. ADS VtSine parameters

3.1.3. Harmonic balance

Circuit performance and load resistance sweep are simulated by the Harmonic balance ADS module.

3.1.3.1. Overview

Harmonic balance is a frequency-domain analysis technique for simulating distortion in nonlinear circuits and systems. It is usually the method of choice for simulating analog RF and microwave problems, since these are most naturally handled in the frequency domain. Within the context of high-frequency circuit and system simulation, harmonic balance offers several benefits over conventional time-domain transient analysis. Harmonic balance simulation obtains frequency-domain voltages and currents, directly calculating the steady-state spectral content of voltages or currents in the circuit. Many

linear models are best represented in the frequency domain at high frequencies. Use the HB simulation to:

- Determine the spectral content of voltages or currents.
- Compute quantities such as third-order intercept (TOI) points, total harmonic distortion (THD), and intermodulation distortion components.
- Perform power amplifier load-pull contour analyses.
- Perform nonlinear noise analysis.

3.1.4. Parameter to sweep

According with the theoretical inductance value, the inductor is swept by the *Parameter to sweep* module.

Generally, sweeps of individual parameters can be performed most efficiently from within many of the simulator dialog boxes themselves. The ability to step through a series of values automatically is incorporated into all the standard simulation controllers. Sweeps can be performed at both the circuit and the system level.

The following parameters are typical candidates for sweep:

- Signal frequency, amplitude, or power
- Bias voltage or current
- Resistance
- Signal path attenuation
- Impedance
- Ambient temperature
- Most component parameters

However, it is possible to combine sweeps of several parameters into a hierarchical sweep plan. By using parameter sweeps, the next actions can be done:

- Find the bias voltage that yields the best mixer conversion gain.
- Find the load impedance that yields the lowest harmonic distortion.
- Simulate a load-pull measurement.
- Simulate the effects of process variations and temperature on circuit performance.

3.2. Simulations with the shunt-inductor matching network

The first simulated set up is L_{shunt} configuration. This configuration consists in an inductor located in parallel between the source and the rectifier. So, the inductor is the element used to match source and load impedance. L_{shunt} simulations will be carried out using the Harmonic Balance module of ADS. It will be done for 50 Ω and 300 Ω source resistance, in a 10 to -10 dBm available power margin and with a HSMS2850 and HSMS2820 rectifiers. Circuit schematic is shown in Fig. 3.3. As can be seen, the antenna is modelled as an AC voltage source with an output resistance of either 50 Ω or 300 Ω. Ideal lumped components are used for the rest with the exception of the diode, where the actual model has been used. The output load is composed by a filter capacitor of 1 nF (C_L) in parallel with a resistive load (R_{L}), which emulates the autonomous sensor to be powered. Note that, in this matching step, input voltage is not amplified.

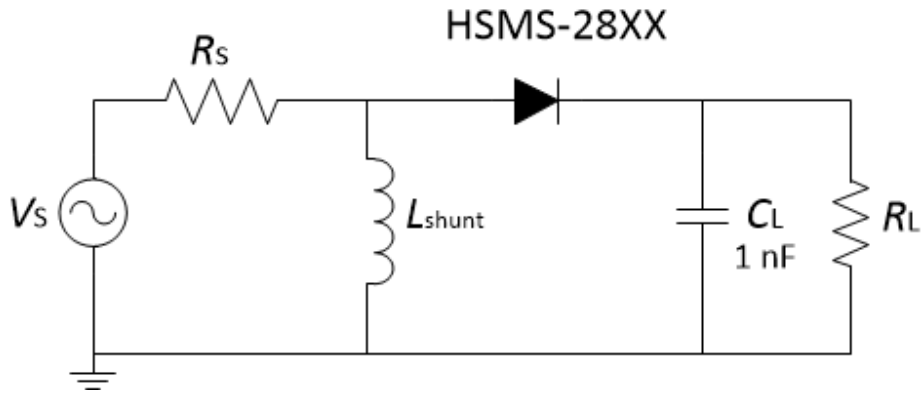

Fig. 3.3. ADS circuit schematic matched through L_{shunt}.

As for L_{shunt} and R_L a parametric sweep will be performed in order to find the best performance in terms of efficiency (η), where:

$$\eta = \frac{P_{\text{L}}}{P_{\text{av}}} \tag{3.1}$$

Being P_{L} is the power dissipated at R_{L}. As commented in chapter 1.4, the inductor has to be designed to compensate the input capacitance of the system. The input capacitance of the system is given by the series combination of the load capacitor and the equivalent capacitance of the rectifier. The linear equivalent circuit model diode chip is:

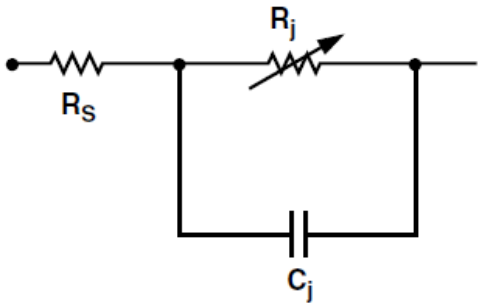

Fig. 3.4. Linear equivalent circuit model HSMS28XX chip.

Whereby C_{j} is the junction capacitance, R_{j} the junction resistance and R_{s} the series resistance. R_{s} is a few of ohms [13], [15] and R_{j} follows the next expression:

$$R_{\text{j}} = \frac{8.33 \cdot 10^{-5} \cdot nT}{I_{\text{b}} + I_{\text{s}}} \tag{3.2}$$

Here is considered a high value of R_{j} in comparison with C_{j} impedance. Therefore, the parallel between R_{j} and C_{j} can be approximated by C_{j}. Thus, the low R_{s} value [13], [15] can be insignificant over C_{j} impedance. A deep studio of rectifier equivalence impedance could be done in future works. Then the input impedance of the rectifier an load can be approximated as a capacitance (C_{in}) in parallel with a resistance (R_{in}). Whereby C_{in} is the series between C_j and C_{L}:

$$C_{\text{in}} = \frac{C_{\text{j}} C_{\text{L}}}{C_{\text{j}} + C_{\text{L}}} \approx C_j \tag{3.3}$$

From HSMS2850 datasheet [13], C_{j} is equal to 0.18 pF. From HSMS2820 datasheet [15], C_{j} is equal to 0.7 pF. In this way, the inductors able to resonate with C_{in} (expression (1.4)) at 868 MHz frequency are:

$$\begin{aligned} L_{\text{shunt}}(2820) &= 48.02\, nH \\ L_{\text{shunt}}(2850) &= 186.8\, nH \end{aligned} \tag{3.4}$$

3.2.1. Simulations with the HSMS2820 diode

Here, the simulations for HSMS2820 rectifier for both source antenna impedance are performed.

3.2.1.1. Simulations with $R_S = 300\ \Omega$

Considering 300 Ω source resistance, the source generator voltage as a function of the available power follows the expression (1.3). These values are valid for a shunt-inductor and L-network matching networks. The source voltages versus the available power are shown.

Available power, $P_{\text{av}}(\text{dBm})$	**Source voltage, $V_{\text{s}}(\text{V})$**
10	4.89
5	2.75
0	1.55
-5	0.87
-10	0.49
-15	0.27
-20	0.15

Fig. 3.5. V_{s} in function of the available power.

Only the efficiency at 10 dBm available power is shown versus R_{L} to display an overview of the process. Then, the maximum efficiency per available power is shown.

3.2.1.1.1. $P_{av} = 10dBm$

The sweep is performed following the next table:

	Load resistance sweep (Ω)	**L_{shunt}sweep (nH)**
Min. value	1	45
Max value	1000	80
Step value	5	1

Fig. 3.6. Sweep values.

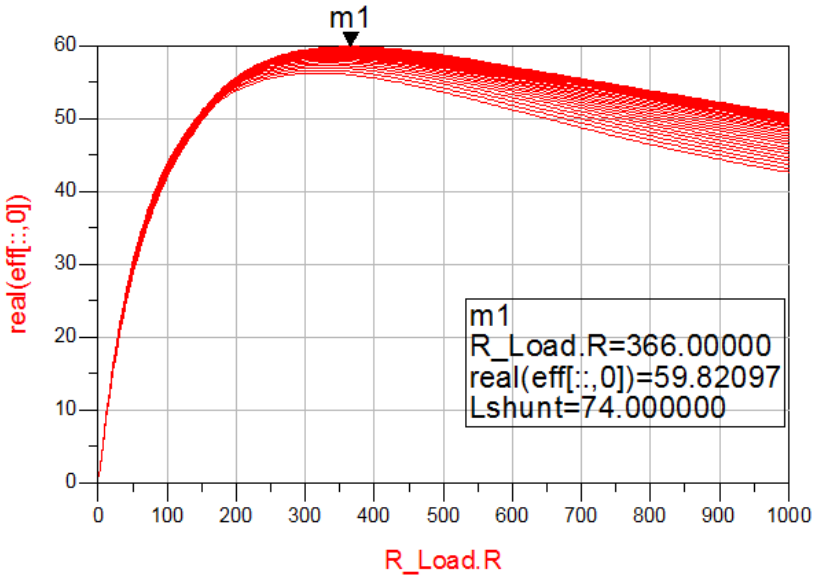

Fig. 3.7. Efficiency vs. R_{L} at 10 dBm.

The maximum efficiency is 59.82 % at 10 dBm input available power for an optimum $R_{\mathrm{L}} = 366\ \Omega$.

3.2.1.1.2. Summary

This section emphasizes the resistance and inductance values that cause the maximum efficiency. The values are shown in the next table:

$P_{av}(\mathbf{dBm})$	$R_L(\Omega)$	$L_{shunt}(\mathbf{nH})$	Eff_{max} (%)
10	366	74	59.82
5	396	63	50.66
0	521	56	38.89
-5	621	50	23.57
-10	941	48	8.51

Fig. 3.8. Maximum efficiency values.

Note that, the value of the inductance does not remain constant as calculated in the expression (3.4). A supposition in this project has been made to explain this fact. Probably the input power variation caused an input capacitance change, so the shunt-inductor changed necessarily.

On the other hand, a graph is proposed in order to show the evolution of the efficiency as a function of the available power:

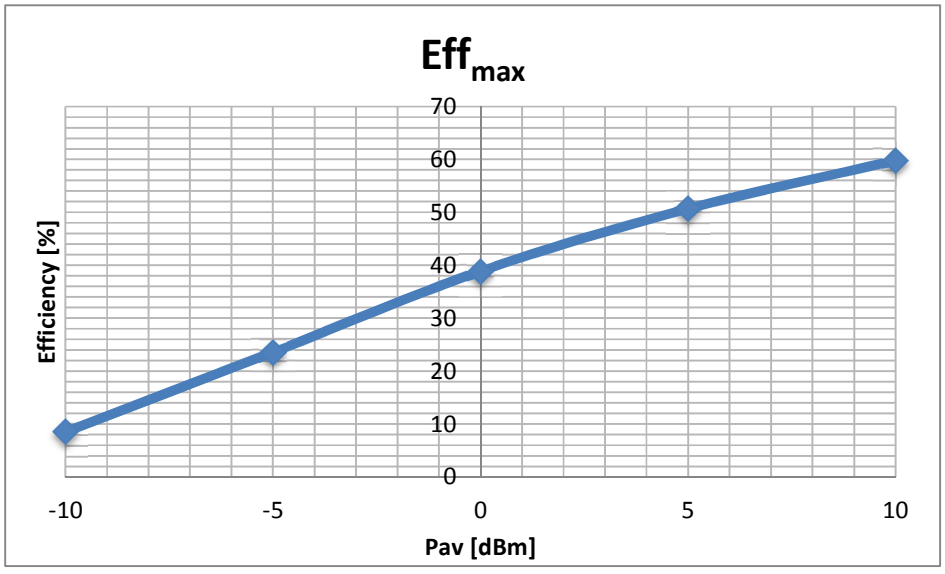

Fig. 3.9. Maximum efficiency at 300Ω.

As can be appreciated, the higher the input available power the higher the efficiency. So, the behaviour is that expected.

3.2.1.2. Simulations with $R_S = 50\ \Omega$

Considering a 50 Ω source resistance, the source generator voltage as a function of the available power follows the expression (1.3). These values are valid for a shunt-inductor and L-network matching networks. The source voltages versus the available power are shown.

Available power, $P_{av}(dBm)$	**Source voltage, V_s (V)**
10	2
5	1.12
0	0.63
-5	0.35
-10	0.2
-15	0.11
-20	0.06

Fig. 3.10. V_s in function of the available power.

Following the same process than section 3.2.1.1 the maximum efficiency per available power is shown.

3.2.1.1.3. Summary

This section emphasizes the resistance and inductance values that cause the maximum efficiency. The values are shown in the next table:

$P_{av}(dBm)$	$R_L(\Omega)$	$L_{shunt}(nH)$	$Eff_{max}(\%)$
10	106	70	35.26
5	116	70	21.77
0	206	65	8.76
-5	611	46	1.07
-10	856	44	0.01

Fig. 3.11. Maximum efficiency values

Note that, the value of the inductance does not remain constant as calculated in the expression (3.4). The supposition to explain this fact is the same than in section 3.2.1.1.2.

On the other hand, a graph is proposed in order to show the evolution of the efficiency as a function of the available power:

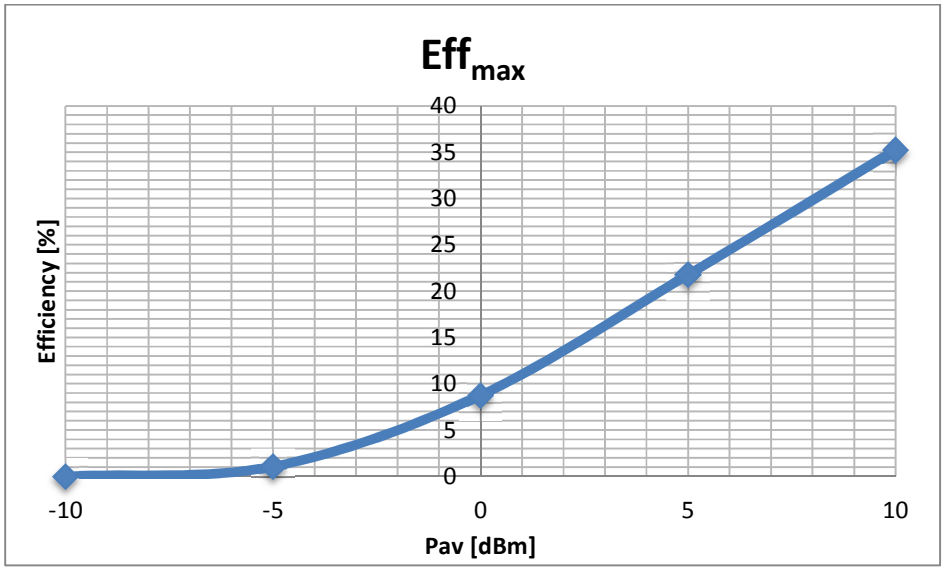

Fig. 3.12. Maximum efficiency at 50.

As can be appreciated, the results of $R_S = 300\Omega$ provide higher efficiency than $R_S = 50\Omega$. This is easily demonstrated through 1.3 expression, which indicates that as higher the antenna impedance as higher the source voltage. Thus, when the voltage at the input of the rectifier is high enough, compare with the dropping voltage, the efficiency is quite high. On the other hand, when the voltage at the input of the rectifier is comparable with the dropping voltage, the efficiency is quite low.

3.2.2. Simulations with the HSMS2850 diode

Here, the simulations for HSMS2850 rectifier for both source antenna impedances are performed.

3.2.2.1. Simulations with $R_S = 300\ \Omega$

Considering 300 Ω source resistance, the maximum efficiency per available power is shown.

$P_{av}(\mathbf{dBm})$	$R_L(\Omega)$	$L_{shunt}(\mathbf{nH})$	$Eff_{max}(\%)$
10	191	190	50.78
5	426	190	56.04
0	471	190	48.98
-5	551	190	38.73
-10	711	190	27.01

Fig. 3.13. Maximum efficiency values.

The simulations have shown that, for L_{shunt} values near or upper than the theoretical resonant inductance (L_{th}), the efficiency remains almost constant:

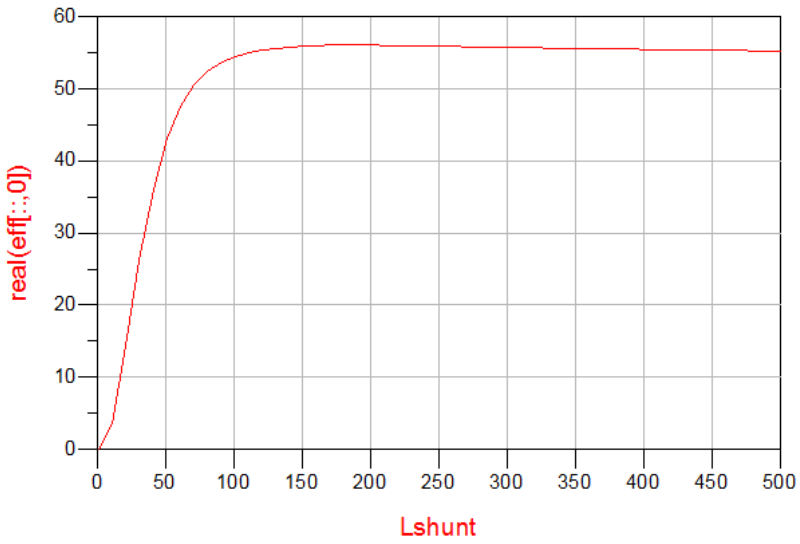

Fig. 3.14. Efficiency vs L_{shunt} at 5 dBm

But seeing the Fig. 3.14 an optimum value of L_{shunt}, close to the theoretical, is found. The efficiency decreasing for upper values of L_{shunt} optimum is slower than the other rectifier.

On the other hand, a graph is proposed in order to show the evolution of the efficiency as a function of the available power:

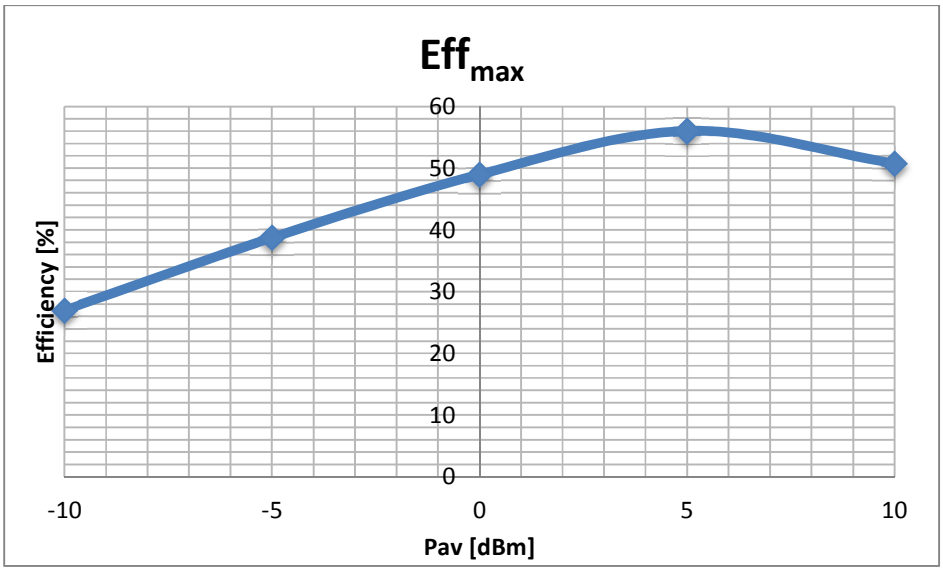

Fig. 3.15. Maximum efficiency at 300Ω.

The expected behaviour would be that the higher the available power the higher the efficiency. But for 10 dBm, the efficiency does not follow the rule because the input voltage at the rectifier is so high and this rectifier has better performance at lower input powers.

3.2.2.2. Simulations with $R_S = 50\ \Omega$

Considering a 50 Ω source resistance, the maximum efficiency per available power is shown.

$P_{av}(\mathbf{dBm})$	$R_L(\Omega)$	$L_{shunt}(\mathbf{nH})$	$Eff_{max}(\%)$
10	146	190	30.68
5	151	190	38.54
0	191	190	16.65
-5	281	190	8.41
-10	571	190	3.12

Fig. 3.16. Maximum efficiency values.

On the other hand, a graph is proposed in order to show the evolution of the efficiency as a function of the available power:

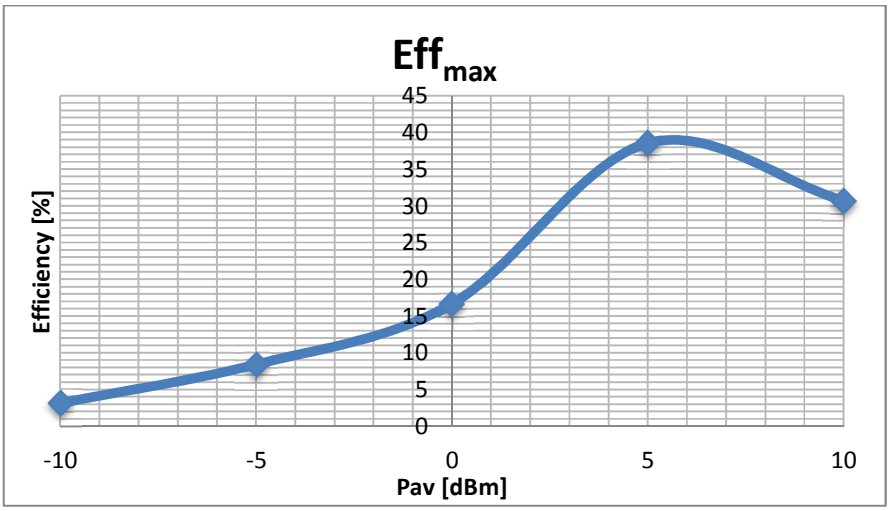

Fig. 3.17. Maximum efficiency at 50.

As for HSMS2820, the results of $R_S = 300\Omega$ provide higher efficiency than $R_S = 50\Omega$. However, the behaviour of HSMS2820 and HSMS2850 rectifier in terms of power is different. HSMS2820 rectifier has better performance at high powers (10 dBm) while HSMS2850 works better at low powers (-10 dBm).

3.3. Simulations with an L-network

In this section, the L_{shunt} matching network is exchanged by a L-network. With this configuration, the input voltage at the rectifier can be boosted. As explained in chapter 2 the gain depends on the relation between impedances (expression (2.27)). Thus, choosing a load impedance many times larger than the source impedance, a voltage at the input of the rectifier that sets the dropping voltage less critical can be achieved. Using the L-network is expected that efficiency increases substantially respects the L_{shunt}. The selected matching network consists in a capacitor (C_{m}) in series with the source and a coil (L_{m}) in parallel with the rectifier and the load. The procedure to obtain the value of C_{m} is described in section 2. As for L_{m} and R_{L} a parametric sweep was performed in order to find the best performance in terms of efficiency (η) (expression (3.1)). As in the case of L_{shunt}, simulations were carried out using the Harmonic Balance module. In this matching network configuration, only the HSMS2850 is used in order to have better performances at low input powers. Fig. 3.13, shows the circuit schematic. Also the antenna is modelled as an AC voltage source.

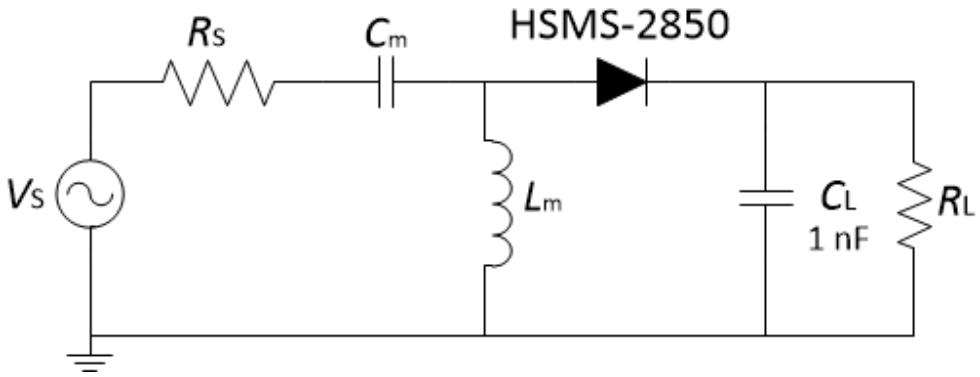

Fig. 3.18. ADS L-network setup

Once the gain is established in a certain load impedance, the values of the C_{m} and L_{m} have to be calculated following the equations (2.14), (2.15) y (2.27):

The frequency used in the system is the same than for L_{shunt} setup which is 868MHz. Also all the components used are lumped except the rectifier which is imported from the library. The L-network simulations will be done for 50 Ω and 300 Ω source resistance, in a -5 dBm to -20 dBm available power margin.

3.3.1. Gain choice

This section wants to show why the chosen voltage at the input of the rectifier has to be 1 V. Only the case with $P_{\mathrm{av}} = -10dBm$ and $R_{\mathrm{S}} = 50\Omega$ has been considered in this section, since the PCB implementation will be performed considering these values. Taking into account the (2.28) expression, the result should tend to zero to maximize the efficiency (100 %). But a trade-off between the voltage at the input of the rectifier and the quality factor has to be considered. Regarding (expression (2.28)):

$$\frac{V_{\mathrm{d}}}{V_{\mathrm{r}}} \cdot 100 \rightarrow 0\,\% \;;\; V_{\mathrm{r}} \rightarrow \infty \tag{3.5}$$

This condition cannot be achieved, however a high V_{R} could be established. Considering $V_{\mathrm{r}} = 10V$ for -10 dBm available power with 50Ω antenna impedance, the resultant gain and quality factor would be:

$$G = 50 \qquad (3.6)$$
$$Q = 99.99$$

The value of Q is too high. Then, the resultant bandwidth becomes very low and consequently, the circuit will be sensible in front of components tolerance. So, a gain value has to be chosen taking into account the Q-Gain trade-off. According with the Q-gain trade-off and L_{eff}, a 6 % efficiency losses is established. Therefore $V_{\text{r}} = 2.5V$, $Q = 25$ and $G = 12.5$ are obtained. Following the formulation described in section 2.1., the L-network has a capacitance and inductor values of:

$$C_{\text{m}} = 0.146\, pF \qquad (3.7)$$
$$L_{\text{m}} = 102.94\, nH$$

Simulating the circuit with this matching network and with a load variable resistance, the maximum efficiency obtained is 70.87 %. In this case, the design has been performed to obtain $L_{\text{eff}} = 6\,\%$, but actually, the efficiency losses are around 30 %. Then, considering the real losses experimented with $L_{\text{eff}} = 6\,\%$, a $L_{\text{eff}} = 20\,\%$ setting is decided. Therefore, $V_{\text{r}} = 0.75V$, $Q = 7.34$ and $G = 3.75$ are obtained. Following the formulation described in section 2.1., the L-network has a capacitance and inductor values of:

$$C_m = 0.493\, pF \qquad (3.8)$$
$$L_m = 50.58\, nH$$

Simulating the circuit with this matching network and with a load variable resistance, the maximum efficiency obtained is 70.12 %. In this case, the design has been performed to obtain $L_{\text{eff}} = 20\,\%$, but actually, the efficiency losses are around 30 %. Finally, an intermediate case with $L_{\text{eff}} = 15\,\%$ is purposed. Thus, a $V_{\text{r}} = 1V$, $Q = 9.95$ and $G = 5$ are obtained. Following the formulation described in 2.1., the L-network has a capacitance and inductor values:

$$C_{\text{m}} = 0.386.\, pF \qquad (3.9)$$
$$L_{\text{m}} = \ 61.7\, nH$$

Simulating the circuit with this matching network and with a load variable resistance, the maximum efficiency obtained is 74.42 %. In this case, the design has been performed to obtain $L_{\text{eff}} = 15\,\%$, but actually, the efficiency losses are around 25 %. So, this matching network provides the best performance.

3.3.2. Simulations with $R_S = 300\ \Omega$

Here, the 10 dBm, 5 dBm and 0 dBm (see Fig. 3.5) cases are not considered, since this project is focused on low power and so the source voltage boost is required. Therefore, simulations for 300 Ω source resistance will be done starting at -5 dBm until -20 dBm. Only the efficiency at -10 dBm available power, the most relevant for the PCB implementation, is shown versus R_L to display an overview of the simulation process. Then, the maximum efficiency per available power is shown.

3.3.2.1. $P_{av} = -10\ dBm$

These are the theoretical values:

Required gain, G	**Input resistance, $R_{in}(\Omega)$**	**Matching capacitance, $C_m(pF)$**	**Matching inductance, $L_m(nH)$**
2.04	4998	0.154	103.4

Fig. 3.19. Theoretical values.

The sweep is performed following the next table:

	Shunt-inductor sweep (nH)	**Load resistance sweep (Ω)**
Min. value	90	1
Max value	105	50000
Step value	1	10

Fig. 3.20. Sweep values.

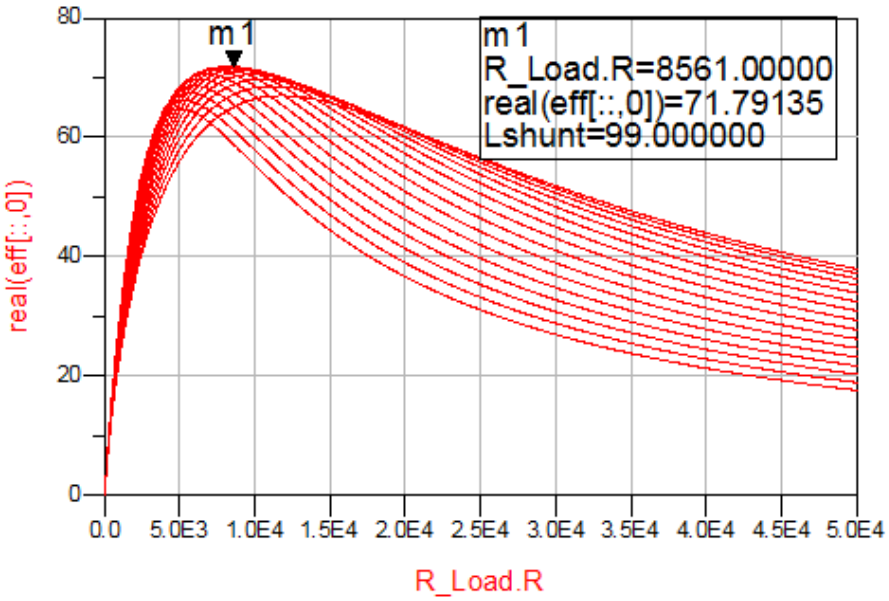

Fig. 3.21. Efficiency vs. R_L at -10 dBm.

Seeing above, the maximum efficiency achieved at -10 dBm is 71.79 % for an optimum $R_{\mathrm{L}} = 8561\ \Omega$. If this maximum efficiency is compared with L_{shunt}configuration at same conditions (27 %), a better performance is achieved for L-network due to the boost of source voltage.

3.3.2.2. Summary

This section emphasizes the resistance and inductance values that cause the maximum efficiency. The values are shown in the next table:

$P_{\mathrm{av}}(\mathrm{dBm})$	$R_{\mathrm{L}}(\Omega)$	$C_{\mathrm{m}}(\mathrm{fF})$	$L_{\mathrm{shunt}}(\mathrm{nH})$	$Eff_{\mathrm{max}}(\%)$
-5	2591	295	75	67.45
-10	8561	154	99	71.79
-15	27781	83.27	123	62.15
-20	47801	45.96	131	33.17

Fig. 3.22. Maximum efficiency values as a function of available power.

On the other hand, a graph is proposed in order to show the evolution of the efficiency as a function of the available power:

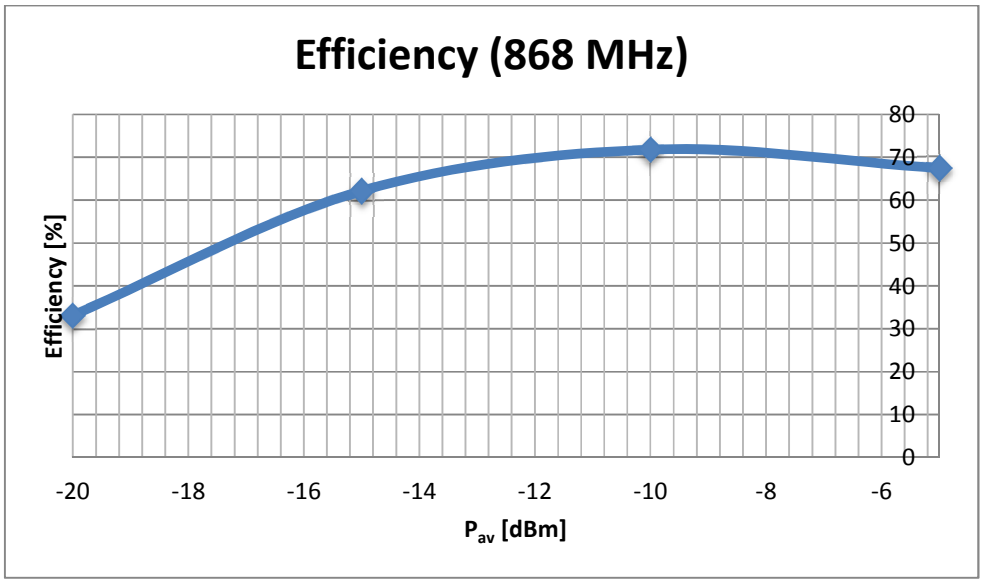

Fig. 3.23. Maximum efficiency at 300Ω.

The figure above shows as higher power as higher efficiency. This rule is fulfilled for all the values except the first one (-5 dBm). This fact is justified because the single diode rectifier used in theses simulations (HSMS2850) which has a better performance at lower powers than -5 dBm.

3.3.3. Simulations with $R_S = 50\ \Omega$

Following the same criteria than in 300 Ω, the simulations will be done for the same available power margin in order to make more exact comparisons. The PCB implementation will be oriented to 50 Ω antenna impedance, so for these simulations all the cases will be shown.

3.3.3.1. $P_{av} = -5\ dBm$

These are the theoretical values:

Required gain, G	Input resistance, $R_{in}(\Omega)$	Matching capacitance, C_m(fF)	Matching inductance, L_m(nH)
2.85	1632	652	41.4

Fig. 3.24. Optimum theoretical values.

The sweep is performed following the next table:

	Shunt-inductor sweep (nH)	Load resistance sweep (Ω)
Min. value	35	1
Max value	55	50000
Step value	1	10

Fig. 3.25. Sweep values.

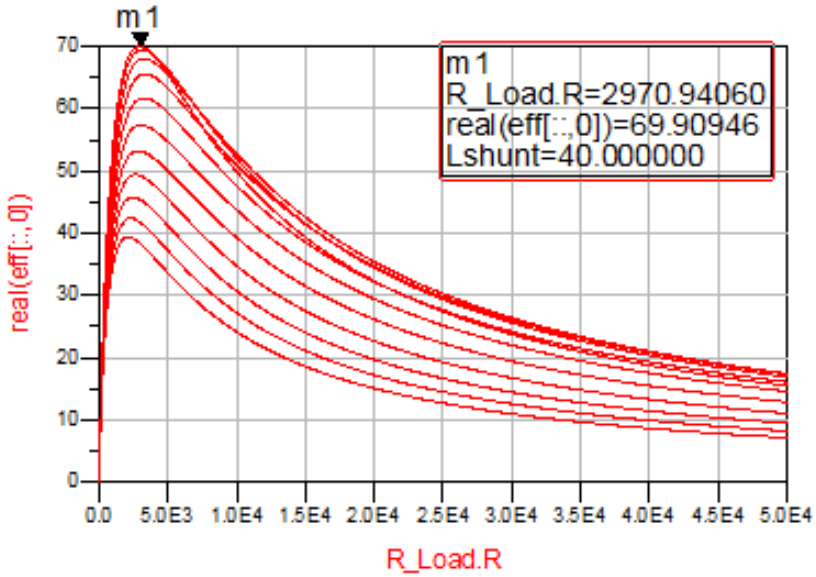

Fig. 3.26. Efficiency vs. R_L at -5 dBm.

The maximum efficiency achieved at -5 dBm is 69.91 % for an optimum $R_L = 2970\ \Omega$.

3.3.3.2. $P_{av} = -10\ dBm$

These are the theoretical values:

Required gain, G	Input resistance, $R_{\text{in}}(\Omega)$	Matching capacitance, $C_{\text{m}}(\text{pF})$	Matching inductance, $L_{\text{m}}(\text{nH})$
5	5000	0.368	61.7

Fig. 3.27. Optimum theoretical values.

The sweep is performed following the next table:

	Shunt-inductor sweep (nH)	Load resistance sweep (Ω)
Min. value	55	1
Max value	65	50000
Step value	1	10

Fig. 3.28. Sweep values.

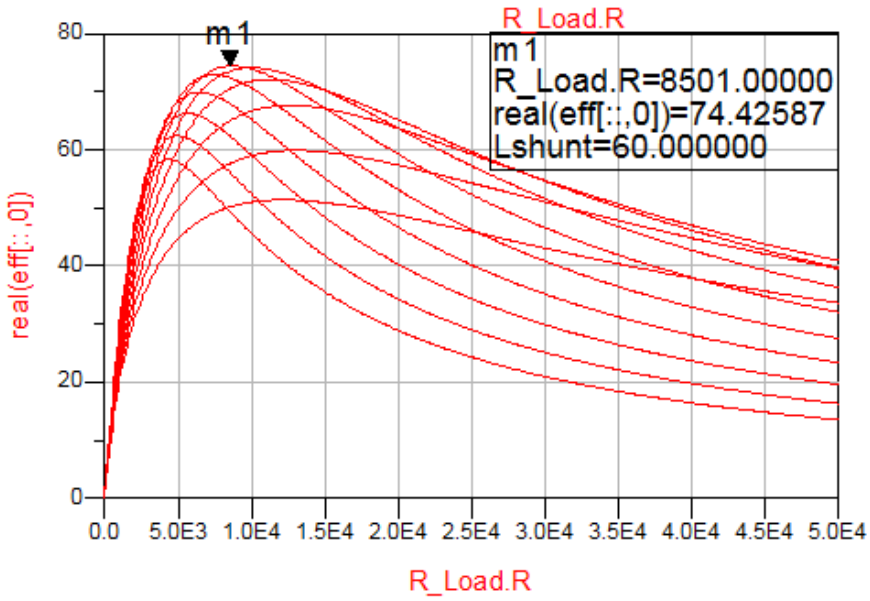

Fig. 3.29. Efficiency vs. R_L at -10 dBm.

The maximum efficiency achieved at -10 dBm is 74.42 % for an optimum $R_{\text{L}} = 8501\ \Omega$..

3.3.3.3. $P_{av} = -15\ dBm$

These are the theoretical values:

Required gain, G	Input resistance, $R_{in}(\Omega)$	Matching capacitance, $C_m(fF)$	Matching inductance, $L_m(nH)$
9.09	16526	202	81.15

Fig. 3.30. Optimum theoretical values.

The sweep is performed following the next table:

	Shunt-inductor sweep (nH)	Load resistance sweep (Ω)
Min. value	75	1
Max value	85	50000
Step value	1	10

Fig. 3.31. Sweep values.

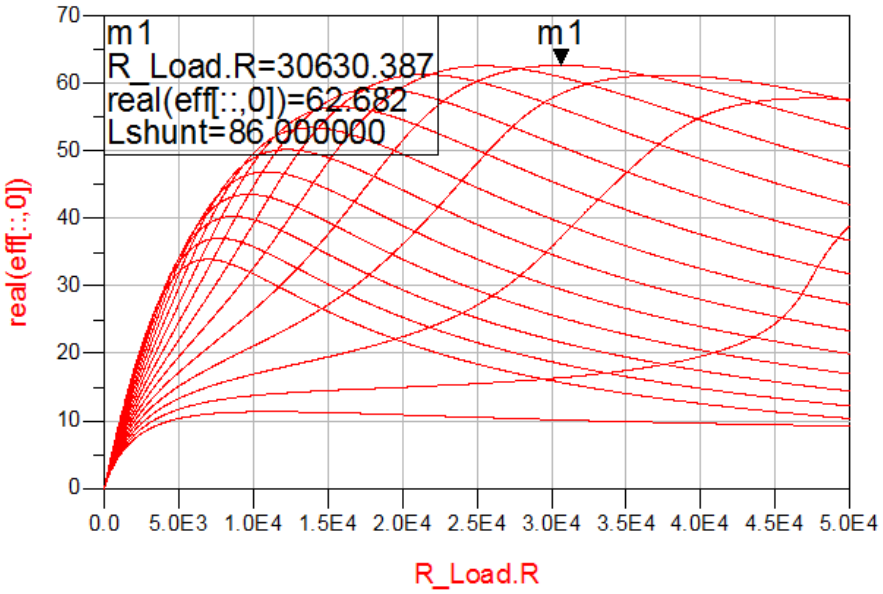

Fig. 3.32. Efficiency vs. R_L at -15 dBm.

The maximum efficiency achieved at -15 dBm is 62.68 % for an optimum $R_{\mathrm{L}} = 30630\ \Omega$.

3.3.3.4. $P_{av} = -20\ dBm$

These are the theoretical values:

Required gain, G	Input resistance, $R_{\mathrm{in}}(\Omega)$	Matching capacitance, $C_{\mathrm{m}}(\mathrm{fF})$	Matching inductance, $L_{\mathrm{m}}(\mathrm{nH})$
15.87	50390	115	113.79

Fig. 3.33. Optimum theoretical values.

The sweep is performed following the next table:

	Shunt-inductor sweep (nH)	Load resistance sweep (Ω)
Min. value	105	1
Max value	115	50000
Step value	1	10

Fig. 3.34. Sweep values.

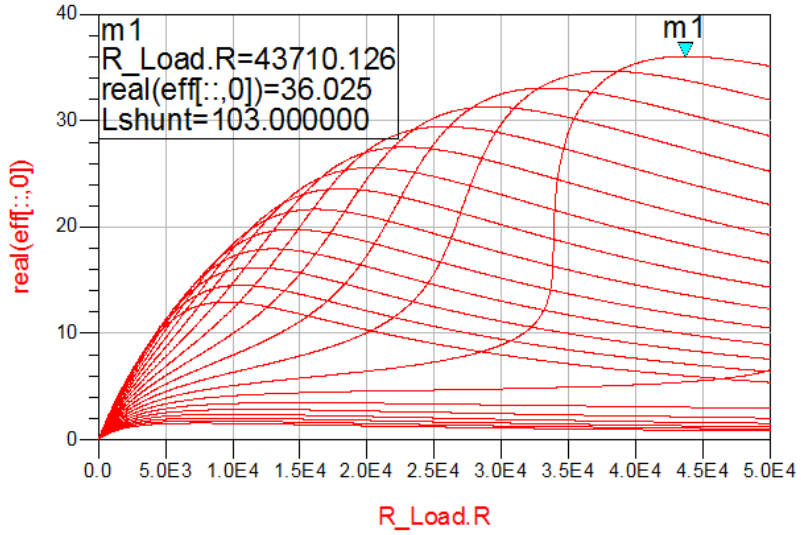

Fig. 3.35. Efficiency vs. R_L at -20 dBm.

The maximum efficiency achieved at -20 dBm is 36.02 % for an optimum $R_{\mathrm{L}} = 43710\ \Omega$.

3.3.3.5. Summary

This section emphasizes the resistance and inductance values that cause the maximum efficiency. The values are shown in the next table:

$P_{\mathrm{av}}(\mathrm{dBm})$	$R_{\mathrm{L}}(\Omega)$	$C_{\mathrm{m}}(\mathrm{fF})$	$L_{\mathrm{shunt}}(\mathrm{nH})$	$Eff_{max}(\%)$
-5	2970	652	40	69.9
-10	8501	368	60	74.42
-15	30630	202	86	62.68
-20	43710	115	103	36.02

Fig. 3.36. Maximum efficiency values as a function of available power.

On the other hand, a graph is proposed in order to show the evolution of the efficiency as a function of the available power:

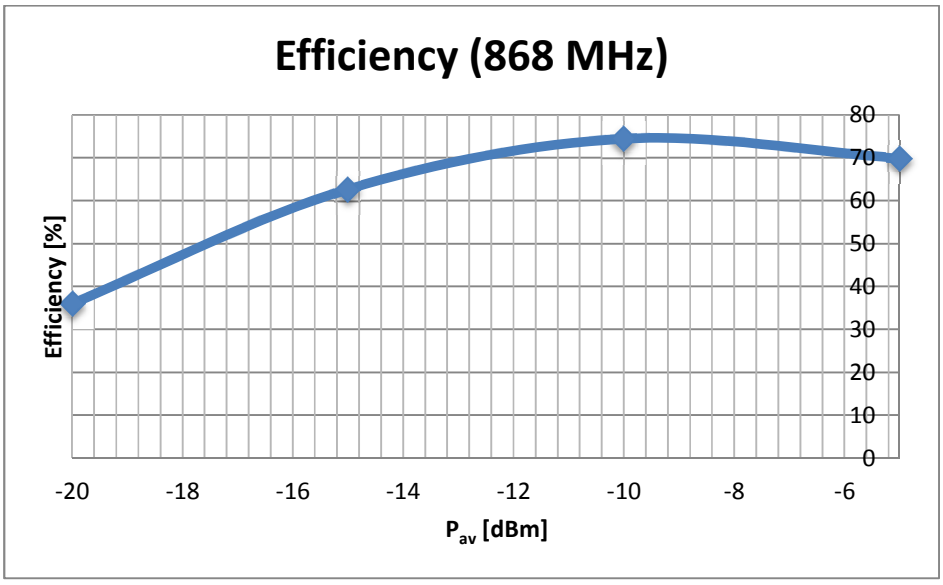

Fig. 3.37. Maximum efficiency at 50 Ω.

The followed pattern by the 50Ω source resistance configuration is the same than 300Ω source resistance. Applying the same conclusion for both source impedances, the single diode rectifier used in theses simulations (HSMS2850) has a better performance at lower powers than -5 dBm. As can be appreciated, the efficiencies obtained for both antenna impedances are similar. This is because the design condition, which is 1V at the input of rectifier.

CHAPTER 4. PCB IMPLEMENTATION AND MEASUREMENTS

The next step before the PCB implementation will be the layout generation. The implementation will be made only for the L-network set up, since it presents better performances. In fact, the -10 dBm configuration presented before is the studied case. In this project is considered that -10 dBm available power represents an enough low value to achieve an efficiency similar to that obtained at high power levels. Here, the problems of transmission the RF signal and the use of commercial components appear. In this way, the circuit must be slightly redesigned to solve these problems.

4.1. RF circuit transformation

First of all, changing the elements of the circuit for elements able to work in RF is mandatory. Conductors will be modified by microstrip lines and junctions by Tees. Several design parameters must be considered for both components.

4.1.1. Microstrip lines design

As explained in section 1.4, microstrip lines design implies material and electrical parameters choice as well as the physical characteristic of the line.

- Material parameters: Dielectric and conductor
- Electrical parameters: Impedance and frequency
- Physical characteristic: Physical length, width, height and thickness.

The available resources at the workplace give FR-4 as the proposed usable dielectric. FR-4 (or FR4) is a grade designation assigned to glass-reinforced epoxy laminate sheets, tubes, rods and printed circuit boards (PCB). FR-4 is a composite material composed of woven fiberglass cloth with an epoxy resin binder that is flame resistant (self-extinguishing). [14]

Commercial software exists in order to design the transmission line. In this project, the TXLine software has been chosen. TXLine works introducing a set of desired parameters and electrical characteristics. Then, software gives the physical characteristics to fulfil the electrical behaviour. Inside the physical characteristics, introducing height and thickness is mandatory, which are provided by the substrate

supplier. To exemplify how the software works, a TXLine screenshot is shown (Fig. 4.1.) with the parameters introduced by the user underlined in red and the parameters calculated by the software underlined in black. The values of the remaining parameters are not taken into account, since they do not affect our design. Phase Constant, Effective dielectric constant and Loss are parameters calculated by the software from the introduced parameters. Electrical length is an editable parameter, but its value is not important as explained in section 1.4.1.2. Note that, GaAs dielectric is selected in Material parameters instead of FR-4. TXLine does not offer the FR-4 option but its characteristics can be edited. In this way, any dielectric type could be chosen.

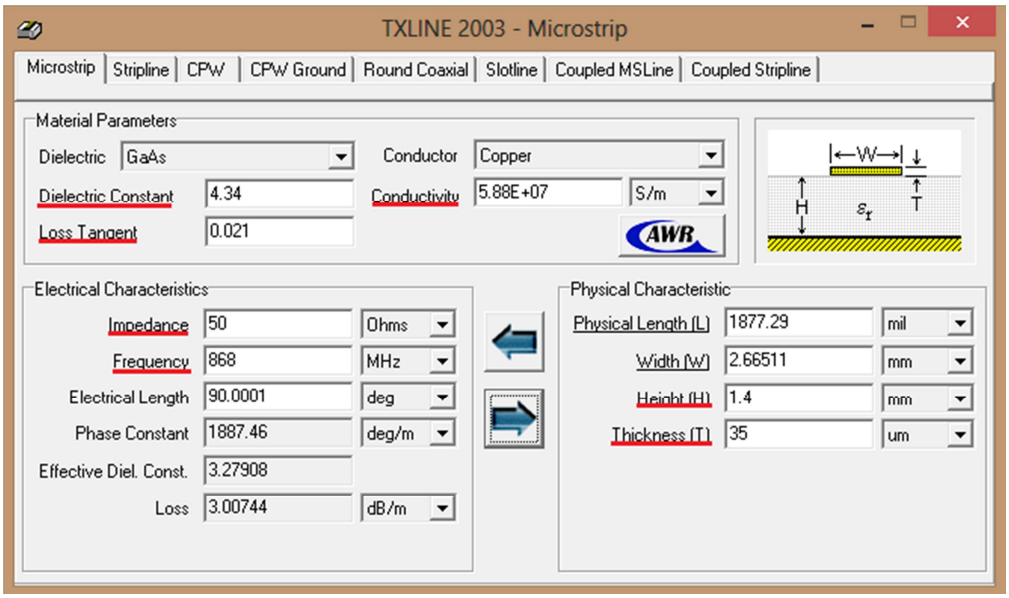

Fig. 4.1. Screenshot from TX- LINE® (National Instruments).

4.1.2. ADS importation from TXLine

Once the transmission line is designed, the parameters obtained can be exportated to the ADS software. Firstly, the established and obtained values in TXLine software must be introduced in substrate ADS module called MSub:

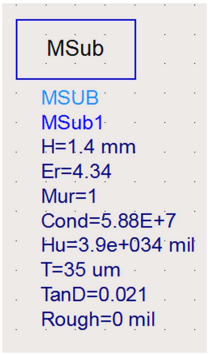

Fig. 4.2. MSub ADS module.

Whereby H_u is cover height, $Mu_r = \mu_r$ is relative permeability and *Rough* is conductor surface roughness. Secondly, the microstrip line has to be configured:

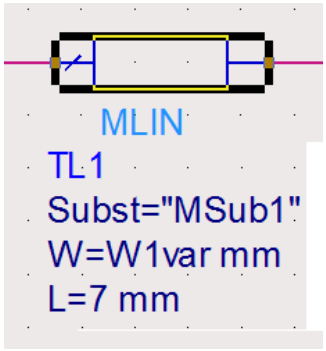

Fig. 4.3. ADS MLIN symbol.

Whereby *Subst* is the substrate defined above, *W* is the width provided by TXLine software and "*L*" the physical length of the line. Note that physical length is not critical, as explained in 1.4.1.2. Thirdly, the same for T parameters:

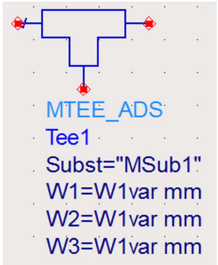

Fig. 4.4. ADS Tee symbol.

Note that $W_1 = W_2 = W_3 = W$, where W has been defined in Fig. 4.4.

4.1.3. Commercial components

The last modification consists in exchanging the almost ideal components to commercial components. Two components will not be exchanged; R_{L}, which is intended to sweep in the prototype and L_{m}, which is the matching network swept component used to match the whole circuit by fixing C_{m}. Taking into account this assumption only the capacitors C_{m} and C_{L} will be exchanged by:

Element	Ideal value	Commercial value	Manufacturer	Model	Encapsulation	Tolerance
$\boldsymbol{C_{\mathrm{m}}}$	0.368 pF	0.4 pF	AVX	ACCU-F Series	0603	A Tolerance, $\pm$ 0.05 pF
$\boldsymbol{C_{\mathrm{L}}}$	1 nF	1 nF	ATC	700 Series	0603	F Tolerance, $\pm$ 1 %

Fig. 4.5. Commercial values.

Manufacturer and model have been decided considering who of them offer the lowest components tolerance. The choice criterion is selecting the commercial component value nearest from a possible commercial value. The 0603 encapsulation is used because it fits properly with the transmission line width.

4.2. Simulation

An ADS picture of the whole circuit used in the simulation is shown:

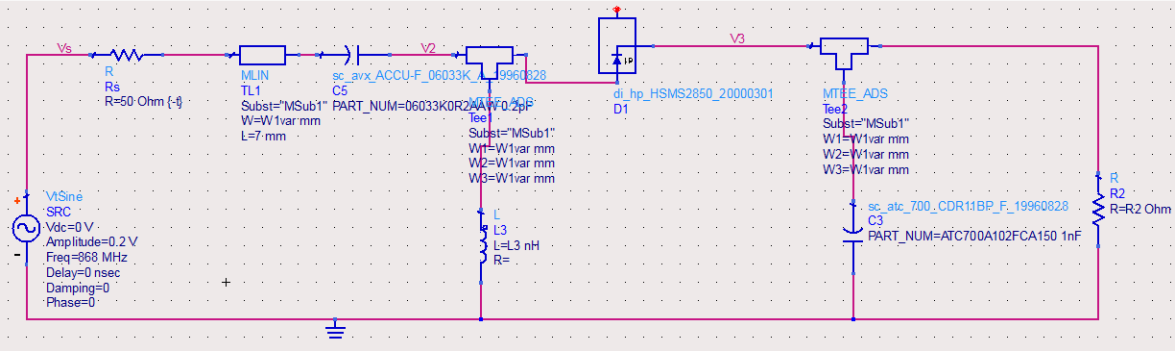

Fig. 4.6. ADS circuit scheme.

The results obtained in the simulations made in section 3.3.3. indicate that -10 dBm available power is a value enough low to exemplify the power remaining in the ambient and hence, a high efficiency is gotten. In addition, 50 Ω source resistance will be used because the worst case condition is considered and the most typical antennas have this output impedance. Therefore, -10 dBm available power and 50 Ω source resistance will be the values used to perform the PCB implementation.

The theoretical values are obtained following the process described in section 2.2.:

Gain, G	**Input resistance, $R_{in}(\Omega)$**	**Matching capacitance, $C_m(\mathbf{fF})$**	**Matching inductance, $L_m(\mathbf{nH})$**
4.55	4152	400	57.96

Fig. 4.7. Optimum theoretical values.

The simulation method follows the same process than in chapter 3. The sweep is performed following the next table:

	Shunt-inductor sweep (nH)	**Load resistance sweep (Ω)**
Min. value	40	1
Max value	50	60000
Step value	1	100

Fig. 4.8. Sweep values.

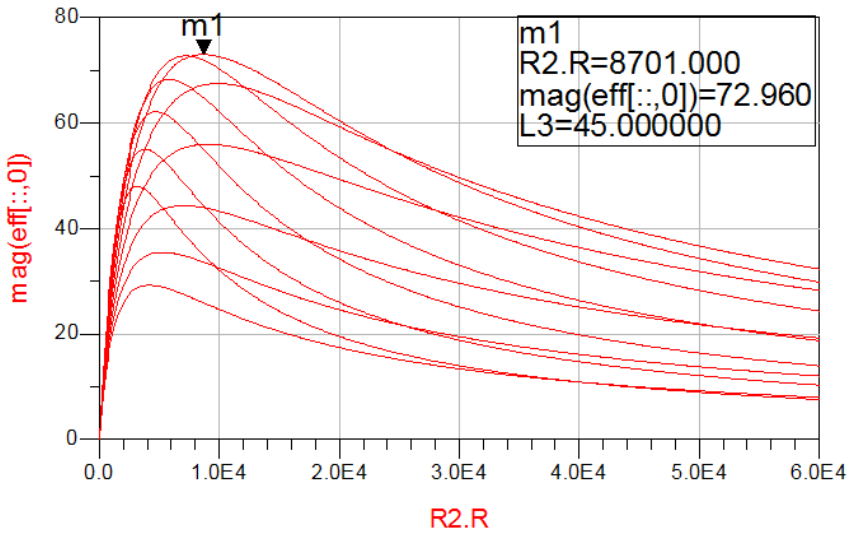

Fig. 4.9. Efficiency vs. R_{L} at -10 dBm.

The maximum efficiency found for $P_{\mathrm{av}} = -10\ \mathrm{dBm}$ in this project is 72.96 % with $C_{\mathrm{m}} = 0.4\ \mathrm{pF}$ and $\mathrm{L}_{shunt} = 45\ \mathrm{nH}$ impedance matching configuration.

4.3. Layout

To print the circuit and obtain the PCB, the layout files generation of the circuit is a must. Layout files of the circuit can be generated by using *Layout > Generate* ADS functionality. However, this functionality does not provide a good layout schematic if the ".dsn" file is not correctly adapted. Deciding in this way, the layout is designed from the beginning.

4.3.1. Substrate definition

First of all, PCB layers must be defined. A standard layout contains three layers: ground, dielectric and conductor. To define the layers disposition, the functionality *Momentum > Substrate > Create/Modify* has been selected:

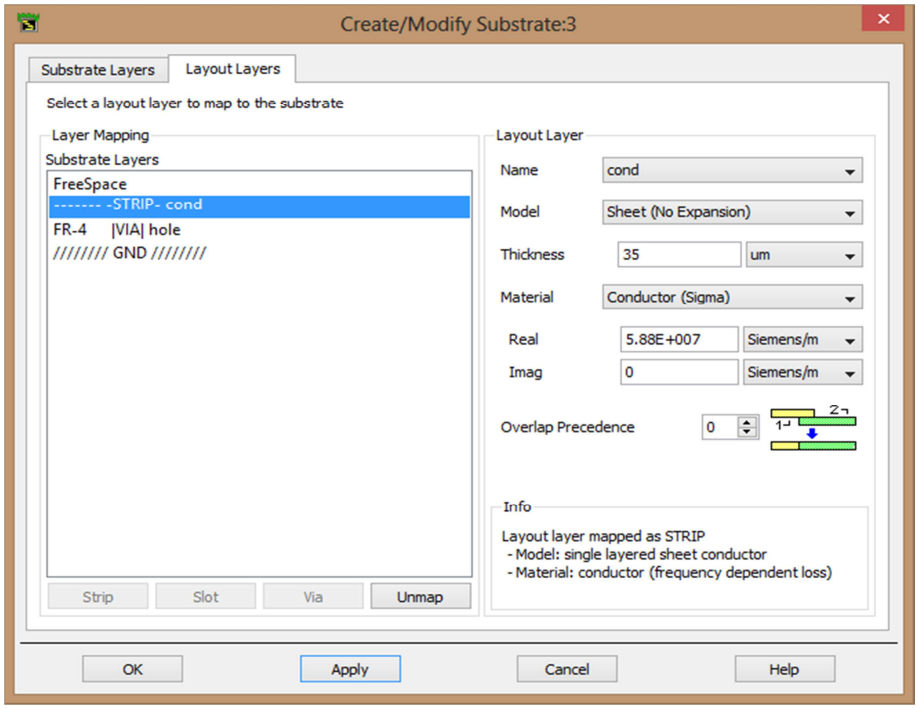

Fig. 4.10. ADS Substrate window screenshot.

The functionality contains two tabs, the first one is where the substrate (FR-4) characteristics are defined and the second one is where the layers characteristics are indicated:

- Ground (GND): not requires for any parameter.

- FR-4:
  - [VIA] Hole: This layer is used to connect the strip conductor and GND layers.
  - Strip conductor: The conductivity, thickness and the model of the conductor are defined in this layer.

- Free space: Any parameter is required.

4.3.2. Microstrip transmission lines definition

When the substrate is defined, the transmission lines definition must be done. It follows the same process than in section 4.1.2. by using the ADS element MLIN. The circuit needs three transmission lines which two of them are TEE elements (the elements used to join components). The first one, at the antenna side, is the most critical, because this

microstrip line impedance has to be equal than that the antenna in order to transfer the maximum power. As explained in section 4.1.2., TEE elements will contain the same width at the three sides, which is the same than in section 4.1.1.

The last step consists in placing all the parts with the correct separation between them. The real components belong to SMD technology, so an encapsulation of 0603 (1.6 mm x 0.8 mm) is selected regarding with section 4.1.3. Considering this data, the parts where the components will be placed must be separated taking into account a portion where the welding is expected.

4.3.3. Vias definition

Another important feature of the layout is the holes definition. Holes are just a vias inside a transmission line, which connect the ground with conductor layers. Holes located in a transmission line transform the line into ground. In addition to the holes, the circuit layout will contain pins vias used to place a variable resistor which will be a potentiometer. The potentiometer will be placed in this set of vias (three) with a separation between them given by the own potentiometer pins. Two of them are connected to ground while the other one to the rectifier. Below the potentiometer pin located in parallel with the rectifier, a portion of the ground layer must be isolated in order to avoid that this pin becomes ground. In this way, the potentiometer will properly work.

4.3.4. S-Parameters

Before the simulation, assembling all the parts and adding some simulation points, which are called ports, is necessary. Ports must be located in the transmission line sides where the components are placed. They are used to obtain the S parameters. Next, a picture of the whole circuit is shown:

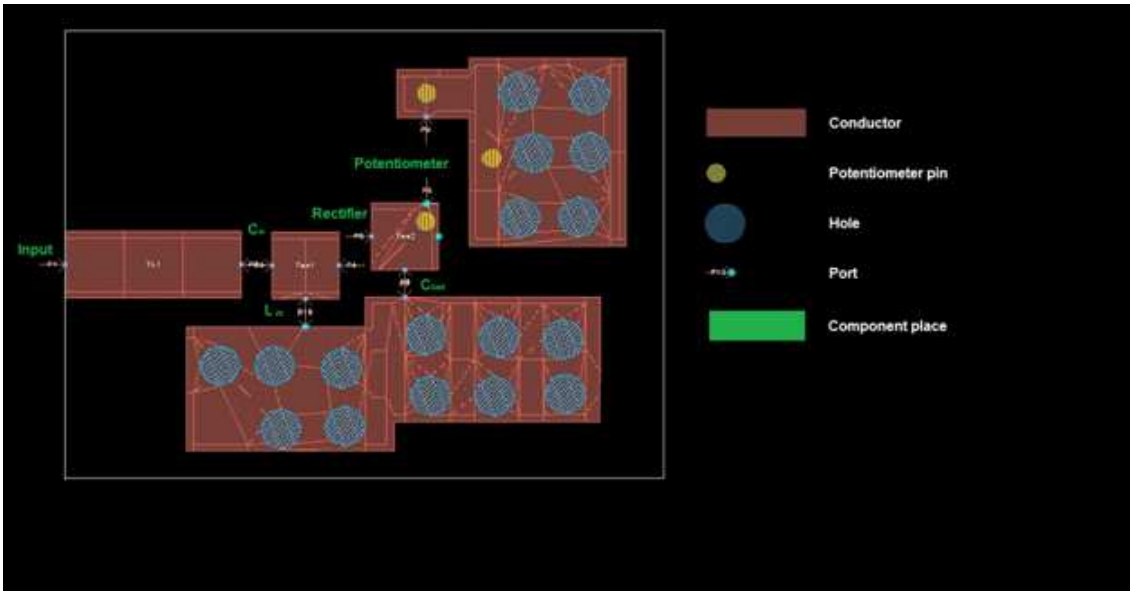

Fig. 4.11. ADS circuit layout.

All the ports are defined as internal except the input port, which is defined as single mode. Once ports are defined, the next step is obtaining the S parameters. These parameters are acquired by accessing at *Momentum* > *Simulation* > *S-parameters*:

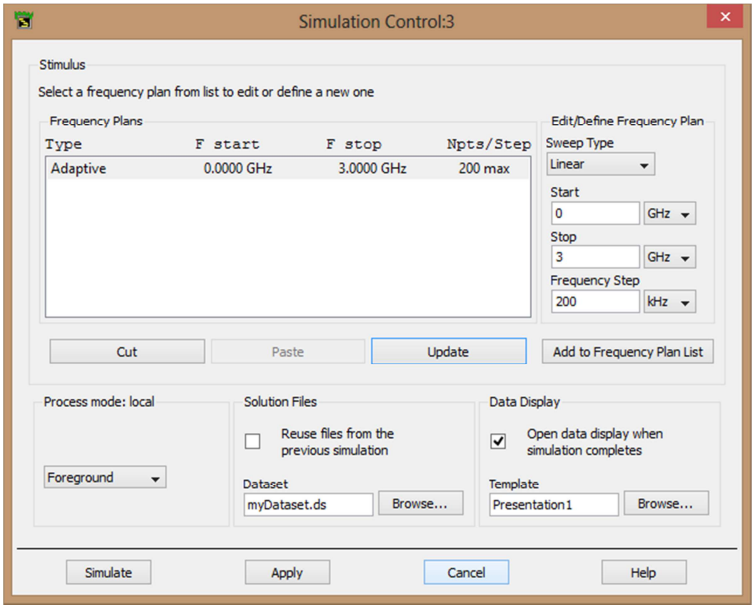

Fig. 4.12. ADS S-Parameters simulation.

The selected frequency plan is defined with a linear sweep type with a range of 0 to 3 GHz in steps of 200 MHz. S Parameters are saved in a database, which will be used in the final simulation.

4.3.5. PCB simulation

With the S parameters, making an accurate simulation of the PCB is possible. Coming back to schematic is needed in order to perform the simulation. Then, a chip with a number of ports equal at the ports number of layout is selected in the palette. This chip is empty; therefore, S parameters must be loaded in the chip in order to emulate the PCB behaviour. Components have to be situated between the same port number than in the layout, since the S parameters are calculated through these ports. The real components used are shown below:

Element	Commercial value	Manufacturer	Model	Encapsulation	Tolerance
C_{m}	0.5 pF	AVX	ACCU-F Series	0603	A Tolerance, $\pm$ 0.05 pF
C_{L}	1 nF	ATC	700 Series	0603	F Tolerance, $\pm$ 1 %
L_{m}	26.6 nH	Coilcraft	0603HS Series	0603	J Tolerance, $\pm$ 5 %
Rectifier	-	Avago Technologies	HSMS2850	-	-
Potentio-meter	1Ω to 50 kΩ	-	-	-	-

Fig. 4.13. Commercial values.

The nominal values of the components have changed significantly. This fact is produced because of two main factors:

1) The transmission lines, layers, holes and vias effects.

2) The components tolerance in agreement with the layout

Evaluating these effects, the optimum values have been found by trial and error near to the theoretical values. These components yield the maximum efficiency. Next, an ADS picture of the circuit is shown:

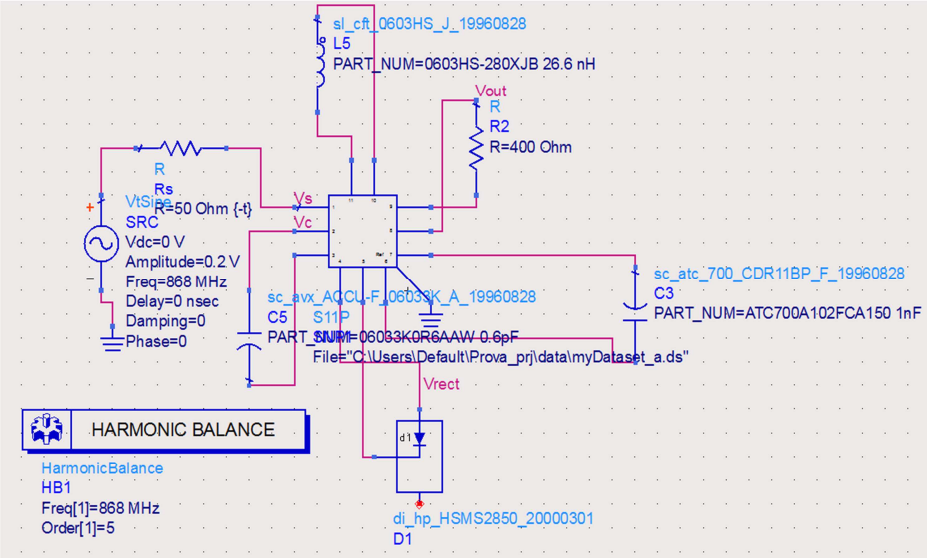

Fig. 4.14. ADS circuit scheme.

The simulation used is Harmonic Balance, which is configured maintaining the same parameters. Also, a sweep in R_{L} is performed to emulate the potentiometer. The results obtained are shown below:

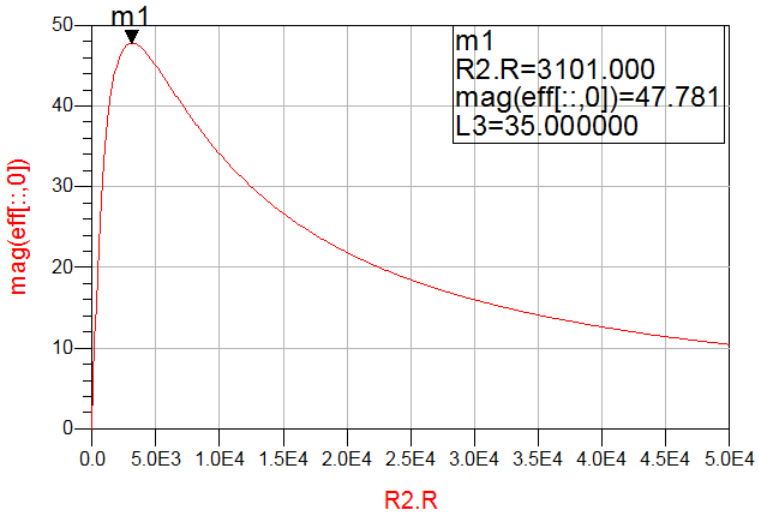

Fig. 4.15. Efficiency vs. R_L at -10 dBm.

The efficiency is plotted versus R_{load}. As can be appreciated, the maximum efficiency is 47.78 % with an optimum $R_L = 3101\,\Omega$. The results achieved in the simulation of the section 4.2 (73 %) are quite higher, since the S parameter characterization was not done and so, the dielectric and conductor effects were not taken into account.

4.3.6. Gerber files

In order to print the PCB, a machine language files generation is required. These files are called Gerber. The number of Gerber files has to be equal to the layout layers. The generated Gerber files are the following:

- Conductor: Contains the transmission lines.
- Holes: Contains the situation of holes.
- Pins: Contains the situation of pins
- Case dimension: Contains the edges of the board.
- Bottom: Contains the bottom layer (ground) of the board.

A picture with all the layout layers is displayed below:

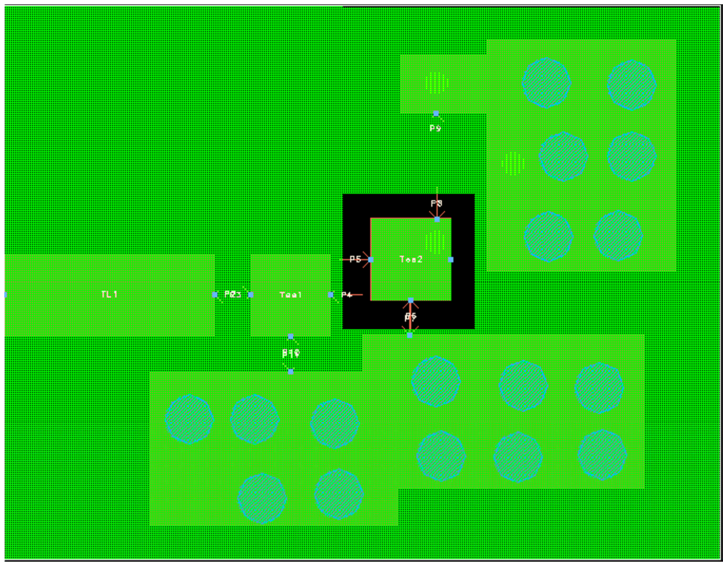

Fig. 4.16. Gerber files generator.

The green layer of the picture above corresponds with the bottom layer. The isolated square belongs to the explanation in section 4.3.3.

4.4. PCB measurements

Finally, with the Gerber files generation, the circuit can be performed. This process is made by a machine and only the human action intervenes when the components are welded in their place. The final PCB circuit is shown:

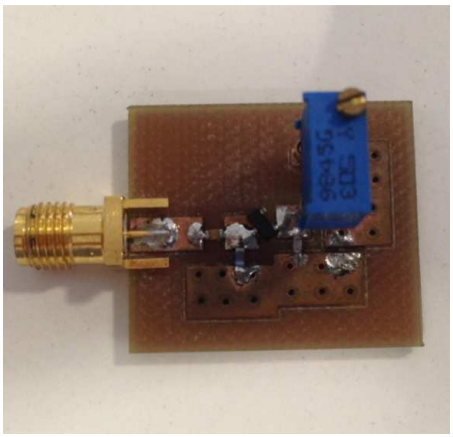

Fig. 4.17. Final PCB prototype picture.

Note that, a SMA connector is welded at the input of the circuit in order to receive the source signal.

4.4.1. Measurement process

The measurement process is composed by three parts:

1) Electronic and RF devices selection.

2) Procedure to achieve the measurements.

3) Results presentation.

4.4.1.1. Electronic and RF devices selection.

These are the devices implied in the measurement process:

Device	Name	Main features
RF signal generator	ROHDE & SCHARZ SMB 100A SIGNAL GENERATOR	BW: [9 kHz - 3.2 GHz] Settling level: [-120 dBm - 18dBm]
Spectrum analyser	ROHDE & SCHARZ FSH3 SPECTRUM ANALYZER	BW: [100 kHz - 3 GHz] Resolution BW = 1 kHz
Multimeter	KEITHLEY 2100 6 ½ DIGIT MULTIMETER	Resolution: 0.1μV Input resistance > 10 GΩ
Coaxial cable	SUHNER SWITZERLAND RG 223U 50±2Ω	Losses: 0.6dB
Connectors	N to SMA	Insertion losses: 0.1 dB

Fig. 4.18. Devices characteristics.

- The RF generator is used to emulate an antenna with an output impedance of 50 Ω.
- Spectrum analyser measures the available RF power.
- Multimeter is used to measure Ohm's law parameters.
- Coaxial cable and connectors join the RF signal generator with the PCB.

4.4.1.2. Procedure to achieve the measurements.

This section details how the measures of the circuit have been taken. Before the measurement chain, the next steps are performed:

1) Cable and connector losses characterization.

2) Input signal adjustment: Considering the cable and connector losses, the RF signal generator power is adjusted to the desired value:

$$P'_{\mathrm{av}}(\mathrm{dBm}) = P_{\mathrm{av}}(\mathrm{dBm}) + L_{\mathrm{c}}(\mathrm{dB}) \tag{4.1}$$

Whereby P_{av} is the desired available power at the input of the circuit (which is measured through the spectrum analyser); L_{c} are the cable and connector losses and $P'_{\mathrm{av}}$is the available power adjusted at the RF signal generator. Also the signal frequency is set.

After that, the measurement chain can be performed following the next steps. A numerical example is given in each step:

1) Load potentiometer adjustment: Using the digital multimeter, the resistance yielded by the potentiometer can be measured and adjusted. Given that the potentiometer range is from 1Ω to 50kΩ, the procedure will consist in increasing the resistance value in steps of 500Ω. Once the potentiometer is adjusted, it can be placed on the circuit:

$$R_{\mathrm{L}} = 2010\ \Omega \tag{4.2}$$

2) RF signal connection to the circuit: the adjusted RF signal is introduced to the circuit through a coaxial cable:

$$P'_{\mathrm{av}}(\mathrm{dBm}) = P_{\mathrm{av}}(\mathrm{dBm}) + L_{\mathrm{c}}(\mathrm{dB}) = -10\ \mathrm{dBm} + 0.7\mathrm{dB} = -9.3\ \mathrm{dBm} \tag{4.3}$$

3) Output voltage measurement: the output voltage is measured with the digital multimeter attaching between ground and potentiometer:

$$V_{\mathrm{out}} = 0.23\ \mathrm{V} \tag{4.4}$$

4) Result recording: the measured output voltage is recorded in a graph editor software:

$\boldsymbol{V_{\mathrm{out}}(\mathrm{V})}$	$\boldsymbol{R_{\mathrm{L}}(\Omega)}$	$\boldsymbol{P_{\mathrm{out}}(\mathrm{W})}$	$\boldsymbol{Eff}(\%)$	$\boldsymbol{P_{\mathrm{av}}(\mathrm{W})}$
0,23	2010	2,6318E-05	26,318408	0,0001

Fig. 4.19. Example values.

5) Graph building.

6) Maximum efficiency point tracking: From the results obtained, the maximum efficiency point is found to check which the optimum load resistance value is.

7) Frequency tuning: Once the maximum efficiency point is obtained, a frequency tuning in this resistance value is made in order to verify if another near frequency provides more efficiency. This step is done because probably the components tolerance has shifted the resonance frequency. Also, the BW is obtained by searching the output voltage values which amplitude has decreased a $\sqrt{2}$ factor

4.4.1.3. Results presentation

Following the procedure in section 4.4.1.2., the results are exhibited.

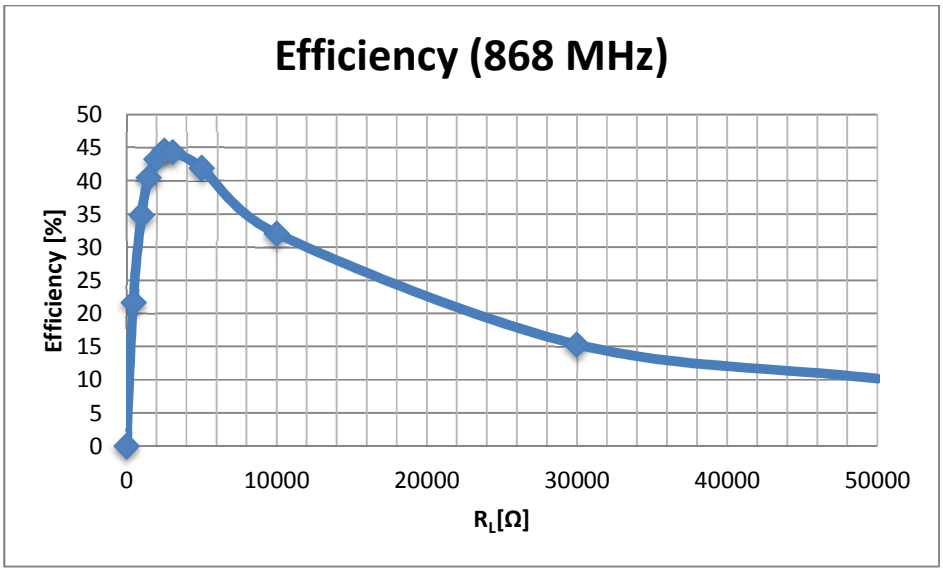

Fig. 4.20. Efficiency vs. R_L at -10 dBm.

The maximum efficiency achieved at 868 MHz is 44.62 % for an optimum $R_{\mathrm{L}} = 2500\ \Omega$. So, experimental results largely agree with simulations. Then a frequency tuning is performed and no different frequency has yielded more efficiency. Even so, a122 MHz bandwidth is obtained. On the other hand, efficiency decreased to 34.5 % and 22.5 % at -15 dBm and -20 dBm, respectively.

4.5. Antenna implementation and measurements

A complementary part of the project has been performed in this section in order to check the harvester performance in front of real antennas. Two antennas have been manufactured at the resonant frequency of the system. The first one acts like a transmitter, which is connected to a RF signal generator. The second one receives the signal emitted by the transmitter and it is connected to the harvester.

4.5.1. Antenna implementation

To learn the process and avoid additional costs, antennas have been fabricated instead of buying to an antenna provider. The manufacturing process is the same for both antennas and it follows the next steps:

1) Ground plane: Especially manufactured with an area enough big to simulate an infinity ground plane in front of the antenna. A N-male connector has been welded in its base in order to receive connections.

2) Antenna wire: A copper wire with a quarter-wavelength length to fulfil the monopole resonance condition:

$$\frac{\lambda}{4} = 0.086\ m \tag{4.5}$$

   Antenna wire is welded at the ground plane centre.

3) Cables and connectors calibration: Cables and connectors are calibrated through a calibrator with 50 Ω terminations. Connections between calibrator and network analyser are done to characterize the cables-connectors pair.

4) Matching verification: Antenna is connected to the network analyser and S parameters are measured. Only S_{11} is evaluated, since S_{11} parameter quantifies the input power that comes back to the source in front of the available power transmitted by the source. Thus, a negative logarithmical value at the resonance frequency is required to S_{11} in order to transfer the maximum input power and so, to check the antenna matching. The S_{11} measurement notices if the maximum matching is centred at the designed frequency. Therefore, an adjustment of the antenna wire length can be done until the maximum matching coincides with the designed frequency. S_{11} parameters for antenna transmitter and receiver screenshots are shown:

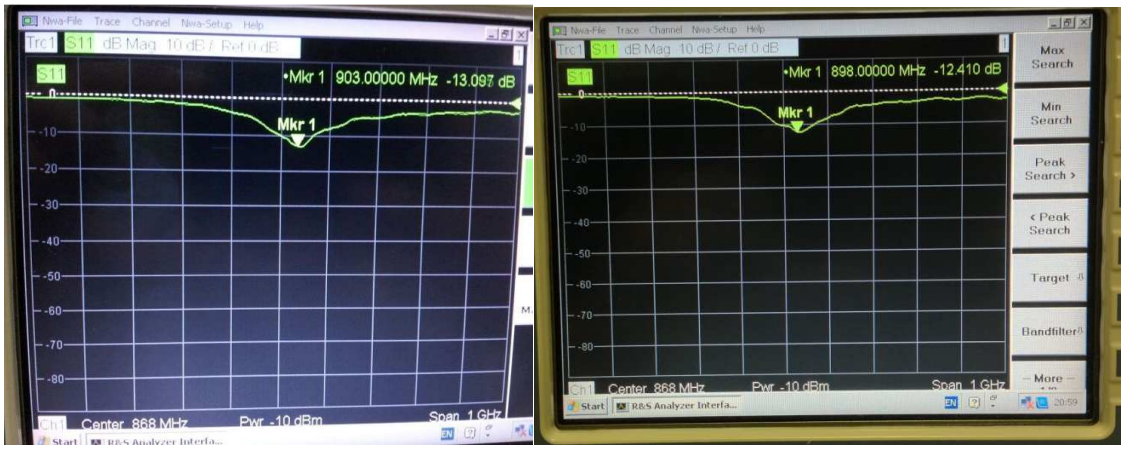

Fig. 4.21. a) S_{11} antenna transmitter. b) S_{11} antenna receiver.

Fig. 4.21 shows S_{11} parameters in a network analyser where cables and connectors have not been calibrated. However a value of S_{11} lower than -10 dBm is enough in order to consider that a good matching has been done.

5) Resonance verification: A second verification can be performed for the antenna design. Through the network analyser, Z_{11}can be displayed in the Smith Chart in order to check if the antenna is resonating. If the antenna is matched at the design frequency, it will not resonate at this frequency because matching and resonance frequency are necessarily different. Therefore, Z_{11} notice that the antenna has a reactive part in series with the antenna resistance at the matching frequency. The PCB has been designed considering a resistive antenna source, so the antenna wire length must be adjusted until resonance is achieved. On the other hand, when resonance occurs, the resistive part of the antenna will not be 50 Ω.

Fig. 4.22. a) Z_{11} antenna transmitter. b) Z_{11} antenna receiver.

4.5.2. Antenna integration to the RF energy harvester measurement

Once the antennas have been characterized, their integration can be done to the RF energy harvester. As commented in section 4.5., the antenna transmitter has been connected to the RF signal generator and the antenna receiver is connected to the input SMA connector of the PCB. The antennas are placed at distance of 1 m in a straight line with LOS (line of sight). Considering the Friis equation in free space, the losses can be modelled as:

$$L_{\mathrm{d}}(\mathrm{dB}) = -10\log\left[\frac{\lambda^2}{(4\pi d)^2}\right] = 31.21\ \mathrm{dB} \tag{4.6}$$

According with expression (4.6), a power level at the RF signal generator must be configured to yield the required input power at the harvester:

$$P_{\mathrm{RF}}\,(\mathrm{dBm}) = P_{\mathrm{av}} + L_{\mathrm{d}} \tag{4.7}$$

Whereby P_{RF} is the power level configured at the RF signal generator. Then, a set of measurements have been done following the procedure described in section 4.4.1. As explained at the point 5 of the section 4.5.1., the series impedance of the antenna changes the nominal value (50 Ω). Therefore, a new optimum R_{L} must be found, that results in 4000 Ω. This load resistance yields a maximum efficiency of 41,85 % at -10 dBm available input power (then, $P_{\mathrm{RF}} = 21.21\,\mathrm{dBm}$). Maintaining the optimum load resistance, -15 dBm and -20 dBm available input power measurements are performed obtaining 29,42 % and 19,73 % maximum efficiency respectively. As can be appreciated, efficiency levels are near in front of that obtained in section 4.4. A little variations are produced since the power at the input of the harvester was not exactly constant due to the radiolink channel.

CONCLUSIONS

A simple matching technique using a L-network has been proposed in order to boost the efficiency for RF harvesters at low power levels. Another matching technique based on a single inductance has been analysed to compare the better performance yielded by the L-network. A theoretical approach in order to find out suitable values of the capacitance and inductance of the L-network has been shown. Consequently, the gain was obtained to boost the input voltage. On the other hand, the inductor matching technique has been approximated by resonance with the input capacitance of the load without producing any voltage amplification. All the simulations have been done with an AC voltage source. For the simple inductance, simulations have shown efficiencies of 3 % for an input power of -10 dBm with ideal components but using the commercial model of the diode rectifier. Simulations for L-network setup have shown efficiencies of 73 % with the same conditions. The results obtained in both matching techniques demonstrate that the input voltage boost to 1V at the input of the rectifier is the key step to achieve a better efficiency at low power levels. In this way, the incorporation of the PCB layout effects to L-network setup is made, and the commercial components decreases the efficiency to below 50 %. Experimental results largely agree with simulations showing an efficiency of 45 % at -10 dBm. Efficiency decreases to 34.5 % and 22.5 % at -15 dBm and -20 dBm, respectively. By tuning the frequency, a 122 MHz bandwidth was obtained. Finally, real antennas have been manufactured in order to measure the harvester performance in a real scenario and 41.85 %, 29,42 % and 19.73 % maximum efficiencies was obtained for -10, -15 and -20 dBm available input power respectively.

REFERENCES

[1] M. T. Penella, M. Gasulla, "Powering Autonomous Sensors: An Integral Approach with Focus on Solar and RF Energy Harvesting", 1st ed. Barcelona: Springer Science+Business Media, 2011.

[2] Chris Bowick, John Blyler and Cheryl Ajluni, "RF Circuit Design," 2nd ed. Burlington: Elsevier Inc, 2008.

[3] M. Pinuela, D.C. Yates, S. Lucyszyn, P. D. Mitcheson, "London RF survey", June 2013 . Available at the web: http://www.londonrfsurvey.org/.

[4] Soltani H. N. and F. Yuan, "A High-Gain Power-Matching Technique for Efficient Radio-Frequency Power Harvest of Passive Wireless Microsystems," *IEEE Trans. Circuits Syst. I, Reg. Papers*, Vol. 57, No. 10, 2685 - 2695, 2010.

[5] Nintanavongsam, P., U. Muncuk, D. R. Lewis and K. R. Chowdhury, "Design Optimization and Implementation for RF Energy Harvesting Circuits," *IEEE J. Emerg. Sel. Topic Circuits Syst.*, Vol. 2, No. 1, 24 - 33, 2012.

[6] Marian, V., B. Allard, C. Vollaire, and J. Verdier "Strategy for Microwave Energy Harvesting From Ambient Field or a Feeding Source," *IEEE Trans. Power Electron.*, Vol. 27, No. 11, 4481 - 4491 2012.

[7] Wikipedia foundation, Inc. "Microstrip", [Online]. May 2013, [July 2013]. Available at the web: http://en.wikipedia.org/wiki/Microstrip

[8] H. A. Wheeler, "Transmission-line properties of parallel wide strips by a conformal-mapping approximation", *IEEE Trans. Microwave Theory Tech.*, vol. MTT-12, pp. 280-289, May 1964.

[9] H. A. Wheeler, "Transmission-line properties of parallel strips separated by a dielectric sheet", *IEEE Tran. Microwave Theory Tech.*, vol. MTT-13, pp. 172-185, Mar. 1965.

[10] H. A. Wheeler, "Transmission-line properties of a strip on a dielectric sheet on a plane", *IEEE Tran. Microwave Theory Tech.*, vol. MTT-25, pp. 631-647, Aug. 1977.

[11] M. Pinuela et. al, *IEEE Trans. Microw. Theory Techn.* (2013).

[12] G. Andia Vera et al., *Proc. IEEE RWS 2010,* pp.61-64.

[13] Avago technologies, HSMS-285x Series datasheet.

[14] Wikipedia foundation, Inc. “FR-4”, [Online]. June 2013, [July 2013]. Available at the web: http://en.wikipedia.org/wiki/FR-4.

[15] Avago technologies, HSMS-282x Series datasheet.

[16] Electronic Communications Committee, “ERC Recommendation 70-03,” ed. Tromso, October 2012.

[17] Nicolas Pillin, “Design of high data rate, passive, far-field RFID tags in CMOS technology”, *École Polytechnique Fédeérale de Lausanne,* 12 March 2010.